UC San Diego

UC San Diego Electronic Theses and Dissertations

Title

Regulation of Cardiac Conduction by Stretch /

Permalink

https://escholarship.org/uc/item/5tr970hw

Author

Pfeiffer, Emily Ross

Publication Date

2013

Peer reviewed|Thesis/dissertation

eScholarship.org Powered by the California Digital Library
University of California

UNIVERSITY OF CALIFORNIA, SAN DIEGO

Regulation of Cardiac Conduction by Stretch

A dissertation submitted in partial satisfaction of the
requirements for the degree Doctor of Philosophy

in

Bioengineering with a Specialization in Multi-Scale Biology

by

Emily Ross Pfeiffer

Committee in charge:

Professor Andrew D. McCulloch, Chair
Professor Ju Chen
Professor Adam J. Engler
Professor Jeffrey H. Omens
Professor Hemal H. Patel

2013

Copyright

Emily Ross Pfeiffer, 2013

All rights reserved.

The Dissertation of Emily Ross Pfeiffer is approved, and it is acceptable in quality and form for publication on microfilm and electronically:

_____

_____

_____

_____

_____
Chair

University of California, San Diego

2013

DEDICATION

To my grandmother

Emily A. Tingley Wilder

TABLE OF CONTENTS

Signature Page iii

Dedication iv

Table of Contents v

List of Abbreviations ix

List of Figures xi

List of Tables xii

Acknowledgements xiii

Vita xvi

Abstract of the Dissertation xviii

Chapter 1 Introduction 1

Introduction 2

Organ-Scale: Cardiac Mechanoelectric Feedback 3

Commotio Cordis 3

Mechanically Triggered Arrhythmias 4

The Bainbridge Response 5

Ventricular Repolarization 6

Myocardial Electrical Properties 6

Cell-Scale: Myocyte Electromechanical Coupling 7

Stretch-Activated Currents 7

Cell-Cell Coupling 8

Membrane Capacitance 10

The Need for Multicellular Tissue-Scale Experiments 10

Cardiomyocyte Cell Cultures 11

Engineered Cardiac Tissue 13
Ventricular Slice and Wedge Preparations 13
Conclusions 14
Acknowledgements 15
References 15
Chapter 2 Stretch-Dependent Electrophysiology in Multicellular Preparations 24
Introduction 25
Physiological Stretch Magnitude 25
Tissue-Scale Multicellular Preparations 26
Stretch Application 27
Methods 27
Microfabricated Substrate 28
Optical Mapping 29
Results 31
Stretch Range 31
Smallest Stretches 33
Largest Stretches 34
Conclusions 35
Acknowledgements 38
References 38
Chapter 3 Caveolae in Stretch-Dependent Conduction Slowing 41
Introduction 42
Methods 43
Animal Models for Tissue Studies 43
Pressure-Loaded Isolated Heart Studies 44

Isolated Heart Optical Mapping 45
Electron Microscopy 46
Stretch of Micropatterned Neonatal Murine Ventricular Myocyte (NMVM) Cultures 47
Optical Mapping of Micropatterned Monolayers 48
Myocyte Patch Clamp 49
Lipophilic Dye 50
Statistics 51
Results 51
Mouse Ventricular Action Potential Propagation in Slowed by Increased Ventricular Filling Pressure Independently of SAC Blockade 51
Conduction Slows Reversibly and Independently of SAC Blockade with Physiological Stretch in Micropatterned Neonatal Mouse Ventricular Myocyte Monolayers 52
Caveolae are Required for Stretch-Induced Conduction Slowing in the Intact Heart and Micropatterned Myocyte Cultures 54
Stretch In Vitro Significantly Increases Whole Cell Capacitance, Independent of SACs 56
Caveolae are Required for Stretch-Dependent Increase in Membrane Capacitance and Time Constant 56
LV Pressure Loading Smoothes Membrane Folds and Reduces Subsarcolemmal Caveolae 57
Sarcolemmal Lipid Density Increases with Stretch in a Caveolae-Dependent Manner 61
Discussion 61

Limitations 63
Acknowledgements 68
References 68
Chapter 4 Role of Desmoplakin in Multicellular Electrophysiology 73
Introduction 74
Methods 75
Cardiomyocyte-Specific Desmoplakin Knockout Mouse Lines 75
Adenoviral Infection of Cardiomyocyte Cultures 76
Optical Mapping 77
Statistical Analysis 77
Results 78
Desmosomal Defects Contribute to Conduction Block 78
Mechanoelectric Uncoupling Influences Beat Rate Variation 80
Loss of Desmoplakin Reduces Connexin 43 Expression, Phosphorylation and Function 81
Conclusions 82
Acknowledgements 83
References 84
Chapter 5 Conclusion 86
Conclusion 87
Acknowledgements 89

LIST OF ABBREVIATIONS

AB	Absolute length
AdCre	Adenoviru-Cre desmoplakin knockdown
AdLacZ	Adenoviru-LacZ desmoplakin control mice
ARVC	Arrhythmogenic right ventricular cardiomyopathy
ASME	American Society of Mechanical Engineers
Cav3 KO	Caveolin-3 knockout mice
C_m	Cell membrane capacitance
CV	Conduction velocity
CV_{max}	Maximum conduction velocity
CV_{min}	Minimum conduction velocity
DSP-cKO	Desmoplakin floxed mice
ECC	Excitation-contraction coupling
ECG	Electrocardiogram
ECM	Extracellular matrix
ECT	Engineered cardiac tissue
IBI	Interbeat interval
ICD	Intercalated disc
LV	Left ventricular
LVP	Left ventricular filling pressure
MβCD	Methyl-β-cyclodextrin
MEF	Mechanoelectric feedback
ML	Membrane length
MSC	Mechanosensitive channel

NMVM	Neonatal mouse ventricular myocyte
nsMSC	Nonspecific cation-selective channels
PC	Pacemaker complex
PDMS	Polydimethylsiloxane
R_m	Cell membrane resistance
ROS	Reactive oxygen species
SAC	Stretch-activated currents
SAN	Sinoatrial node
SiCS	Stretch-induced conduction slowing
T_m	Cell membrane electric time constant
WT	Wild-type

LIST OF FIGURES

Figure 2.1: Micropatterned PDMS promotes alignment of cardiomyocytes 29

Figure 2.2: Combined apparatus for biaxial stretch of micropatterned neonatal cardiomyocytes and optical mapping of cell membrane potential permits study of conduction through multi-cellular preparations 31

Figure 2.3: Conduction speeding and slowing with stretch depends more on stretch magnitude than on conduction or stretch direction 32

Figure 2.4: Conduction speeding is observed with small stretch 34

Figure 2.5: Conduction slowing is observed with large stretch 35

Figure 3.1: Conduction slows with stretch in hearts and cells 53

Figure 3.2: Stretch-activated channel block does not affect slowing 54

Figure 3.3: Caveolae depletion reduces conduction slowing 56

Figure 3.4: Cell membrane capacitance increase coincides with conduction slowing 58

Figure 3.5: Ultrastructure rearrangement coincides with conduction slowing 60

Figure 3.6: Membrane area fluorescence coincides with conduction slowing 61

Figure 4.1: Desmoplakin facilitates uniform conduction 79

Figure 4.2: A spiral wave is observed in a DSPKO culture 80

Figure 4.3: Desmoplakin facilitates uniform beat rate 81

Figure 4.4: DSPKO cultures retain mechanical but not gap junctions 82

LIST OF TABLES

Table 2.1: Ratio of loaded to initial conduction velocities of all groups measured..... 33

ACKNOWLEDGEMENTS

The content of Chapter 1 is almost identical to sections of a manuscript scheduled for publication in the Journal of Biomechanical Engineering, a publication of the American Society of Mechanical Engineers (ASME), with minor revisions and formatting changes for this dissertation. The authors and title of the submitted manuscript are as follows: Pfeiffer, E.R.,* Tangney, J.R.,* J.H. Omens, A.D. McCulloch, 2014. Biomechanics of cardiac electromechanical coupling and mechanoelectric feedback. Journal of Biomechanical Engineering.

Chapter 2 adapts a figure from the following manuscript scheduled for publication: Pfeiffer, E.R.,* Tangney, J.R.,* J.H. Omens, A.D. McCulloch, 2014. Biomechanics of cardiac electromechanical coupling and mechanoelectric feedback. Journal of Biomechanical Engineering. An image is also adapted from the Online Supplement of a manuscript in preparation for publication in *Circulation Research*. Besides this, the content of Chapter 2 is original. The author would like to thank Jennifer Stowe, Kyle Buchholz, Katie McNall, Justin Tan, Tammy Soo-Hoo and Tik-Chee (Jenny) Cheng for their assistance, as well as Adam Wright, Barbara Murienne, and Amy Hsieh for their technical legacies.

Chapter 3 is an almost exact reproduction of a manuscript in preparation for publication. The title and authors of the manuscript are as follows: E.R. Pfeiffer,* A.T. Wright,* A. Edwards, J.C. Stowe, K. McNall, J. Tan, I. Niesman, H.H. Patel, D.M. Roth, J.H. Omens, A.D. McCulloch. Caveolae in stretch-dependent cardiac conduction slowing. We gratefully acknowledge the contribution of peptide GsMTx-4 from Dr. Fred Sachs in Buffalo, NY, and technical assistance of Barbara Murienne, Michael Yang, Kyle Buchholz, Tammy Soo-hoo, Tik-Chee “Jenny” Cheng, and Mathivadhani Panneerselvam, and the animal management of Selma Garcia and others in the laboratory of Professors Roth and Patel and

VA San Diego Hospital vivariums, as well as in the UCSD vivariums. Microfabrication of molds for PDMS patterning was carried out in the Nano3-Calit2 cleanroom facility at UCSD.

Chapter 4 contains text and figures almost identical to two manuscripts, with formatting changes for this dissertation, along with additional original text and figures (Fig. 4.4). One has been accepted for publication and is in press at *Human Molecular Genetics* which is a publication of Oxford University Press. The citation is: Lyon, R.C.,* Mezzano, V.,* A.T. Wright, E. Pfeiffer, J. Chuang, K. Banares, A. Castaneda, K. Ouyang, L. Cui, R. Contu, Y. Gu, S.M. Evans, J.H. Omens, K.L. Peterson, A.D. McCulloch, F. Sheikh, 2013. Connexin defects underlie arrhythmogenic right ventricular cardiomyopathy in a novel mouse model. Human Molecular Genetics. The second manuscript is in preparation for submission to *Ciculation Research*, and the working title and authors are: V. Mezzano, A.T. Wright, R.C. Lyon, E. Pfeiffer, Y. Gu, N. Dalton, S.M. Evans, K.L. Peterson, A.D. McCulloch and F. Sheikh. Desmosomal junctions are necessary for synchronized action potential propagation in the mouse cardiac pacemaker complex.

The content of Chapter 5 is original. The author would like to thank Professors Andrew McCulloch and Jeffrey Omens for guidance in this project and Adam Wright, Valeria Mezzano and Andy Edwards for discussions of mechanoelectric feedback, intercellular coupling, and electrophysiology.

This work was done with the kind assistance of Jennifer Stowe and Jeff Van Dorn, in addition to those listed above. Gratitude is due to the advice of optical mapping predecessors including Adam Wright and Barbara Murienne. Collaborators Valeria Mezzano and Indroneal Banerjee worked in the development of the knockout lines the author has tested, and brought good cheer to these and various projects. Mathi Panneerselvam, Selma Garcia, and others in the Roth and Patel lab and in the UCSD vivariums provided animal husbandry to which this

project is indebted. The author would like to thank her committee, Andrew McCulloch, Jeff Omens, Ju Chen, Adam Engler, and Hemal Patel, for constructive guidance in this project.

This work was supported by National Institutes of Health (NIH) National Heart, Lung, and Blood Institute (NHLBI) grant number 5P01HL46345-12, and used computational clusters at the National Biomedical Computation Resource supported by the NIH National Center for Research Resources (NCRR) program grant P41 RR 08605. Microfabrication was performed in the Nano3 cleanroom facility of the California Institute for Telecommunications and Information Technology. ERP was supported by the National Science Foundation (NSF) Graduate Research Fellowship under grant number DGE1144086.

The author would like to thank the Siebel Foundation for their support in the form of a Siebel Scholarship and the Siebel Scholars community.

VITA

2003- 2007 Massachusetts Institute of Technology
Bachelor of Science, Mechanical Engineering
Minor, Biomedical Engineering
Senior Research Thesis, Tissue Engineering Laboratory

2007-2009 University of California, Davis
Master of Science, Biomedical Engineering
Howard Hughes Integrating Medicine into Basic Science Fellow
National Science Foundation Graduate Research Fellow
Graduate Researcher, Biofluids and Cellular Mechanics Laboratory

2010-2013 University of California, San Diego
Doctor of Philosophy, Bioengineering
Specialization in Multi-Scale Biology
Interfaces Graduate Training Program Fellow
Siebel Scholar
Graduate Researcher, Cardiac Mechanics Research Group

TEACHING EXPERIENCE

Massachusetts Institute of Technology

Course Grader, Department of Mechanical Engineering
Mechanics of Materials II. Professor M. Boyce. Spring 2007

University Of California, Davis

Teaching Assistant, Department of Biomedical Engineering
Biomaterials. Professor A. Revzin. Spring 2008
Biotransport Phenomena. Professor K. Leach. Winter 2008

University Of California, San Diego

Teaching Assistant, Department of Bioengineering
Cell and Tissue Engineering. Prof. S. Varghese. Fall 2013
Numerical Analysis for Multi-Scale Biology. Professor A. McCulloch. Winter 2013
Biotechnology Laboratory. Professor M. Micou. Fall 2010
Bioengineering Laboratory. Professor J. Omens. Spring 2010

PUBLICATIONS

Peer-Reviewed Research Articles

[In Preparation] **Pfeiffer, E.R.,*** Wright, A.T.,* A. Edwards, J. Stowe, K. McNall, J. Tan, I. Niesman, H. Patel, D. Roth, J.H. Omens, A.D. McCulloch, 2014. Cellular mechanisms of stretch-dependent cardiac conduction slowing.

[In Preparation] V. Mezzano, A.T. Wright, R.C. Lyon, **E. Pfeiffer,** Y. Gu, N. Dalton, S.M. Evans, K.L. Peterson, A.D. McCulloch and F. Sheikh, 2014. Desmosomal junctions are necessary for synchronized action potential propagation in the mouse cardiac pacemaker complex.

[In Press] Banerjee, I., J. Zhang, T. Moore-Morris, **E. Pfeiffer,** K. Buchholz, A. Liu, K. Ouyang, M. Stroud, L. Gerace, S.M. Evans, A. McCulloch, J. Chen, 2014. Targeted ablation of Nesprin 1 and Nesprin 2 from murine myocardium results in cardiomyopathy, altered nuclear morphology and inhibition of the biomechanical gene response. PLOS Genetics.

[In Press] Lyon, R.C.,* Mezzano, V.,* A.T. Wright, **E. Pfeiffer**, J. Chuang, K. Banares, A. Castaneda, K. Ouyang, L. Cui, R. Contu, Y. Gu, S.M. Evans, J.H. Omens, K.L. Peterson, A.D. McCulloch, F. Sheikh, 2013. Connexin defects underlie arrhythmogenic right ventricular cardiomyopathy in a novel mouse model. Human Molecular Genetics.

Morgan, J.T., **E.R. Pfeiffer**, T.L. Thirkill, G. Peng, H.N. Fridolfsson, G.C. Douglas, D.A. Starr, A.I. Barakat, 2011. Nesprin-3 regulates endothelial cell morphology, perinuclear cytoskeletal architecture, and flow-induced polarization. Molecular Biology of the Cell, Vol. 22, pp. 4324-4334. PMCID: PMC3216658.

Tam, B.K., J.H. Shin, **E. Pfeiffer,** P. Matsudaira, L. Mahadevan, 2009. Calcium regulation of an actin spring. Biophysical Journal, Vol. 97, pp. 1125-1129. PMCID: PMC2726317.

Pfeiffer, E., S.M. Vickers, E. Frank, A.J. Grodzinsky, M. Spector, 2008. The effects of glycosaminoglycan content on the compressive modulus of cartilage engineered in type II collagen scaffolds. Osteoarthritis and Cartilage, Vol. 16, pp. 1237-1244. PMID: 18406634.

Peer-Reviewed Review Articles

[In Press] **Pfeiffer, E.R.,*** Tangney, J.R.,* J.H. Omens, A.D. McCulloch, 2014. Biomechanics of cardiac electromechanical coupling and mechanoelectric feedback. Journal of Biomechanical Engineering.

Peer-Reviewed Conference Proceedings

Pfeiffer, E., S. Case, J. Lesko, J. Moore, K. Verghese, J. Bicerano, H. Pham, 2004. Lifetime prediction of glass fiber/DERAKANE 411-350 composites. ANTEC Technical Papers, Vol. 3, pp. 3020-3024.

ABSTRACT OF THE DISSERTATION

Regulation of Cardiac Conduction by Stretch

by

Emily Ross Pfeiffer

Bioengineering with a Specialization in Multi-Scale Biology

University of California, San Diego, 2013

Professor Andrew D. McCulloch, Chair

It is well established that cardiac electrophysiology can be altered by changes in mechanical loading of the heart, through processes of *mechanoelectric feedback (MEF)*. However, the cellular mechanisms and particular strain dependence of these processes have not been determined, partly due to the difficulty in assessing complex mechanical and electrophysiological phenomena in active cardiac tissue, and also to challenges in linking

observations in single cells to organ-level effects. To circumvent these challenges, there is need for electrophysiological studies multicellular platforms with capability for precise, physiologic mechanical loading. In this dissertation, biaxial stretch of micropatterned cardiomyocyte preparations is employed in conjunction with electrophysiological measurement, particularly via optical mapping of changes in membrane potential as well as by patch clamp recording, to discover how mechanoelectric interactions at the cell level may give rise to stretch-dependent alterations in cardiac conduction. Chapter 1 introduces cardiac mechanoelectric feedback starting with the clinical and tissue-scale observations, describing candidate cellular mechanisms and discussing the need for multicellular experiments to bridge the gap between single-cell and whole-organ experiments. Chapter 2 describes a multicellular system for testing electrophysiology under biaxial loading, and reports data from a range of stretch magnitudes. Chapter 3 probes cellular mechanisms for conduction slowing at large physiologic loads, and demonstrates that slowing is due to caveolae-dependent increases in cell membrane capacitance. Chapter 4 utilizes the system to test a transgenic murine model of clinical arrhythmia for conduction block and interbeat variability, demonstrating the capability of the system in examining multicellular electrophysiological phenomena that develop on a spatial scale reflecting human tissue.

Chapter 1

Introduction

Introduction

It is well known that the heart depends on electrical depolarization to trigger mechanical contraction, but mechanical perturbations have also long been seen to affect cardiac electrophysiology.[1,2] The well-studied process by which myocyte electrical activation leads to mechanical contraction is known as excitation-contraction coupling (ECC), while the lesser-known process by which a mechanical alteration influences cardiac electrical activity is referred to as mechanoelectric feedback (MEF). This chapter introduces MEF phenomena, which are manifested at cellular and the whole heart scales. While observations of MEF have been made separately in single cells and in intact tissue, in many cases it remains to be shown which cell mechanisms underlie particular whole heart phenomena.

At the scale of the whole heart, MEF has been fairly well characterized and is known to be altered in various diseases or states of altered contractility, such as electromechanical dyssynchrony. In the whole heart, abnormal sequences of ventricular electrical depolarization adversely affect mechanical contraction and are a major complication when pump function is compromised by heart failure.[3] Extensive studies have been conducted to understand the cellular mechanisms of ECC, while MEF has been studied to a lesser extent. For example, it is now well recognized that dysregulation of intracellular calcium cycling, which is central to ECC, is a major cause of contractile dysfunction in heart failure regardless of the specific heart failure etiology,[4 5] however, the underpinning mechanisms of MEF are currently debated.[2]

Although MEF has been studied separately at the myocyte and whole heart scales, our ability to integrate and translate cellular and molecular mechanisms to *in vivo* physiological

and pathophysiological phenotypes is still limited and the problem is inherently difficult. Ventricular mechanics *in vivo* are highly nonhomogeneous, and arrhythmias depend not only on cellular dynamics but on intercellular coupling, action potential propagation and three-dimensional myocardial structure. Contributing to the paucity of integrative understanding in this field is the comparative scarcity of suitable homogeneous multi-cellular preparations and high-fidelity measurement techniques for investigating tissue-scale myocardial mechanoelectric interactions under well-controlled and readily manipulated conditions. This chapter reviews the state of knowledge of cardiac MEF at the whole organ and single cell scales, and concludes by surveying promising preparations and techniques for investigating these mechanoelectric interactions at the multi-cellular tissue scale.

Organ Scale: Cardiac Mechanoelectric Feedback

Whole heart studies of cardiac mechanoelectric feedback have focused primarily on the mechanisms by which alterations in hemodynamic loading or focal mechanical stimuli can modulate atrial or ventricular electrophysiology and lead in some cases to arrhythmia.[2] Acute changes in mechanics of the ventricles can affect cardiac electrophysiology. Blows to the chest, altered hemodynamic loading, or regional changes in synchrony may have the effect of altering myocardial stretch or pressure loading prior to or during electrical activation. These abnormal mechanical loading situations have been observed to disrupt or distort normal cardiac excitation, and in some cases lead to life-threatening arrhythmias.

Commotio Cordis

Classical studies in cardiac physiology first identified MEF at the organ scale well over 100 years ago.[6] Reports of *commotio cordis* date to the 19th century and possibly earlier. *Commotio cordis* is a rare cause of ventricular fibrillation often resulting in sudden cardiac death initiated by a localized precordial impact that is not sufficiently strong to cause mechanical damage to the heart or surrounding organs. As recorded in the US *Commotio Cordis* Registry, the rate of survival has improved over recent decades, associated with increased workplace safety and bone health, such that incidence is now most common in youth athletics. Survival of these events has been improved by faster response times and availability of an on-site automated external defibrillator. There remains a greater risk of mortality when *commotio cordis* occurs during noncompetitive rather than competitive sports, or in African Americans.[7,8] A condition for fatality is that the chest blow occurs during a vulnerable window preceding the electrocardiogram (ECG) T wave.[9] Recruitment of stretch-activated channels during this period is thought to augment repolarization, increasing dispersion of repolarization and promoting ventricular tachycardia,[7,9] a mechanism supported by computational models.[10] While perhaps the most dramatic, *commotio cordis* is by no means the only pathophysiological example of MEF.

Mechanically Triggered Arrhythmias

Intrinsic mechanical pulses and perturbations can trigger arrhythmias or extrasystoles, and may be especially important in diseases where wall mechanics become altered such as ischemia and heart failure. Transiently increased hemodynamic loading of failing ventricles has been observed to give rise to extrasystolic beats and ventricular tachycardia.[11,12] In a positive counterexample, precordial thump or precordial percussion offers a rapid though low

efficiency method for resuscitation of a victim of witnessed cardiac arrest, though the window for benefit versus harm is small.[13,14,15,16]

The Bainbridge Response

Changes in circulatory pressures have a well-known effect on heart rate. First described in 1915, the "Bainbridge response" describes an increase in heart rate under increased venous, but not under arterial, pressure.[17] Increases in venous return are thought to be sensed *via* stretch receptors in the left and right atria, and transmitted via the vagus nerve to the autonomic nervous system, which rebalances vagal and sympathetic stimulation to the sinoatrial node (SAN) causing an increase in heart rate.[2,18] Unloading below normal levels during hypotension, anesthesia or hemorrhage can result in heart rate decrease and is sometimes termed the "reverse Bainbridge response".[18] However, the Bainbridge effect operates in counterbalance with a slowing in heart rate following rise in arterial pressure, mediated by the baroreceptor and autonomic system. Perhaps due to this counterbalance, the Bainbridge effect is known to be strongest in the species of first discovery (dog). While rate increase is also present in humans and other primates, the net effect is reversed in small mammals.[2,18] Some reports suggest the baroreceptor response can also dominate the Bainbridge response in humans.[19] However, Bainbridge responses are thought to contribute to "physiological" respiratory sinus arrhythmias, modulating blood flow and promoting oxygen uptake.[2] A non-autonomic, cellular mechanism for alterations in heart rate due to perturbations of cell mechanics is tested in **Chapter 4**.

Ventricular Repolarization

The Q-T interval of the ECG, a measure of the delay between ventricular depolarization and repolarization, has been observed to lengthen, and the T-wave to flatten, when ventricular contraction occurs rapidly against a reduced afterload, in animal tissue preparations and in the human heart.[20,21] Commonly, this affect is attributed to changes in action potential duration that lead to dispersion of the repolarization gradient, though the nature of these changes is unsettled and is likely dependent on heart rate.[22,23,24,25,26]

Myocardial Electrical Properties

Additionally, changes in ventricular conduction dependent on hemodynamic load may also contribute to ECG-perceived changes in ventricular repolarization, by delaying the timing of depolarization globally, or offsetting it within a region. Experiments in intact and perfused rabbit hearts have shown conduction slowing with ventricular volume loading, a change which would increase apparent ventricular repolarization time.[26,27] Experiments in a variety of tissue preparations have yielded acceleration, deceleration, or biphasic changes in conduction velocity under several modalities of tissue stretch.[25,27] Conduction acceleration and deceleration under a linear gradient of biaxial stretch is explored in greater detail in **Chapter 2**. Such electrophysiological changes may contribute to susceptibility to reentrant arrhythmia in tissue regionally affected by disease or dyssynchrony.[14,23,24,27,28] Alterations in ion currents may explain the conduction changes observed in stretched tissue, although experiments showing no effect of stretch-activated channel blockers in tissue suggest otherwise.[26,27] Simulations based on these experiments suggest that this slowing may be linked to increased

cell membrane capacitance with tissue stretch.[27,29] The role of these cellular mechanisms in conduction slowing effects is tested in **Chapter 3.**

Cell Scale: Myocyte Electromechanical Coupling

The primary origins of cardiac MEF are in the myocyte, though there is some evidence that fibroblasts are mechanosensitive and do influence action potential propagation. Myocyte mechanoelectric coupling is the process of a cell experiencing mechanical stretch that ultimately alters its action potential. While organ-scale examples of cardiac MEF have been documented and defined, most are not clearly linked to cellular mechanisms outside the autonomic nervous system. One source of this gap in understanding is that cardiac electrophysiology arises from the collective behavior of a population of cells situated in a dynamic mechanical and electrical tissue environment. Electrical activation is achieved through a sequence of ionic currents acting in concert, and alterations in individual currents or ion channels are not easily distinguished, or understood in relationship to interacting currents. Likewise for currents through cell-cell gap junctions and the electrical source-sink interactions surrounding electrotonic loading of passive tissues. The changing nature of cell and tissue electrical properties within a mechanically, biochemically, and electrically dynamic environment are also unclear. For these reasons, many of these effects have been initially studied at the single-cell level or within computational models in order to establish a foundational understanding of their functions. Current understanding of some of these components is summarized here.

Stretch-Activated Currents

Various ionic currents have been proposed to be mechanosensitive in cardiomyocytes, thus producing stretch-sensitive electrophysiological responses, however the effect of these currents in healthy and diseased cardiac function is unclear. While nonspecific cationic, K^+-selective, and Cl^--selective mechanosensitive channels (MSCs) have been identified in various preparations, most cardiac myocyte studies to date have focused on the nonspecific cation-selective channels (nsMSCs).[2,30] The most specific blocking agent used to study these channels is GsMTx-4, a peptide derived from tarantula venom, which is thought to embed in the membrane around nsMSCs such as TRPC6 channels, reducing transmission of membrane tension and mechanosensitive opening of the channels.[31,32,33,34,35] Also commonly used are the rare earth element gadolinium (Gd^{3+}), which broadly affects cationic and anionic MSCs, and cationic antibiotics such as streptomycin, though both have technical disadvantages when compared with GsMTx-4.[2,30,33]

If TRPC6 channels are indeed mechanosensitive, their upregulation in stretch and disease, and effects on Ca^{2+} handling may prove to be important players in MEF.[32,36,37] Computational simulations have suggested a role for nsMSCs in heart rate acceleration and deceleration due to stretch described above, and experimental evidence in SAN tissue using GsMTx-4 is in agreement.[2,38] Computational models and experiments studies suggest a role for nsMSCs in stretch-induced ectopic ventricular contractions, repolarization shortening, and rate-dependent restitution of action potential duration.[22,39,40,41]

Cell-Cell Coupling

Electrochemical communication between cardiomyocytes occurs primarily through connexon channels made up of connexin proteins localized at gap junctions usually within an

intercalated disc joining two cells via mechanoelectrical couplings. These gap junctions afford low resistance current flow between cells, with relative conductivity determined by the constituent connexin isoforms, which are expressed with cell type- and tissue-specificity varying throughout the atria, ventricles, and conduction system.[42,43,44,45,46] Cardiac conduction is thus dependent on the integrity of mechanical junctions between cells, provided by desmosomal proteins such as desmoplakin, tested in **Chapter 4**, and alterations in connexin expression due to disease.[45,47,48,49] Connexon mechanosensitivity in cardiac cells is unknown, although increased conductivity with stretch has been shown in other cell types.[50] Mechanical loading increases expression of gap junction proteins through hypertrophy processes, which can lead to an increase in conduction velocity.[51,52] Alterations in cardiac mechanics via electrical stimulation and heart failure have also been observed to promote gap junction remodeling, increasing susceptibility to arrhythmia.[49,53,54]

Additionally, conductivity may be enhanced by field or electrotonic coupling throughout cardiac tissue. Conduction may be fostered at the peri-nexus region surrounding gap junction plaques through field coupling boosted by $Na_v1.5$ channel enrichment near connexins.[55] Models suggest that ephaptic, or field coupling to surrounding passive tissue could be important in propagation of electrical signals through the myocardium, beyond classical cable model representations.[56,57,58] These findings underscore that changes in cell membrane configuration, observed to occur with stretch, could play an important role in mechanosensitivity cardiomyocyte electrophysiology.[27, 59 , 60 , 61] An electrotonic effect of coupling between cardiomyocytes and cardiac fibroblasts has been demonstrated, in experiments and in simulations.[62,63,64,65] Both fibroblast-mediated slow conduction through myocyte-free regions, and a role in MEF for mechanosensitivity of cardiac fibroblast membrane potential have been suggested, and both often labeled as

arrhythmogenic.[7,66,67,68,69,70] Interestingly, one of the proposed mechanisms for cardiac myofibroblast alterations of cardiac conduction is via forces exerted by the myofibroblasts on the cardiomyocytes, leaving open the possibility of MEF within the cardiomyocytes.[71]

Membrane Capacitance

Beyond affecting constituent channels and junctions, changes in cell membrane configuration with stretch may alter fundamental electrical properties such as capacitance.[59] Although there have been few studies of mechanical effects on myocyte membrane capacitance,[72,73] indirect evidence in intact tissue preparations has implicated changes in membrane capacitance in stretch-induced changes in action potential conduction velocity, as described above.[27] There is some evidence for membrane capacitance increase with membrane tension in other cell types.[72,74] Increased membrane capacitance could be expected to lower excitability and slow conduction of activation through the myocardium, promoting arrhythmia as discussed above. However, a connection between this cellular property and organ-level phenomena remains to be demonstrated. This question is explored further in **Chapter 3**.

The Need for Multicellular Tissue-Scale Experiments

The previous sections have discussed MEF at the cellular and organ levels. Studying these phenomena at the cellular scale helps elucidate the mechanisms involved, but this information does not translate well from the single cell to the whole heart, simply due to the experimental conditions of single cell preparations. Preparations at the spatial scale of tissue can help translate the MEF discoveries made in single cell experiments to the whole heart.

Many physiologically interesting phenomenological observations of MEF have been made through studies of clinical and *in vivo* responses, Langendorff-perfused intact hearts, and whole muscle preparations, while in parallel, complex mechanisms are gradually becoming known at the subcellular and single cell levels. However, the specific cellular mechanisms for many organ-level observations remain elusive, as do the role of particular cellular mechanisms when in concert with the organ. Though there is extensive knowledge and detailed mathematical models of the electrophysiology of single cardiac myocytes in a wide variety of species, arrhythmias are complex, whole-organ, spatio-temporally dynamic phenomena that depend on multi-cellular interactions and cannot be understood based solely on single cell data. Conversely, the whole heart is three dimensional and inhomogeneous, and it is not yet possible to simultaneously map three-dimensional mechanics and electrophysiology throughout the intact heart, much less to perturb them in a well-controlled manner. Effects of interstitial fluids and changing myocardial mechanics (such as fiber orientation) may complicate observations made in whole organ or muscle preparations.

The following sections summarize several different multi-cellular preparations that have been used for studying MEF. These approaches promise to help better integrate the cellular and molecular mechanisms of mechanoelectric feedback with the whole organ physiology of ventricular electromechanical interactions.

Cardiomyocyte Cell Cultures

One concern regarding single cell experiments is that techniques for stretching isolated adult cardiomyocytes are technically quite difficult, and coupling these techniques with electrophysiological study present a difficult hurdle.[75] Depending on the scientific

question, there is interest in testing isolated adult cells as singles, doublets, or as slices or strips of tissue.[54,76,77,78] Still, precise but population-level electrophysiological studies of electrically coupled cells under precise and physiological mechanical strain conditions remains challenging.

Over the years, improved techniques for microfabrication of patterned surfaces and polymer chemistry have been put to work to engineer culture conditions that closely resemble native myocardium. While classical cell culture presents a cell body/substrate stiffness mismatch that typically has deleterious effects on cell development and morphology, softer polymer substrates have been found to optimize cardiomyocyte maturation in culture.[79,80,81] However, soft substrates often preclude experiments imposing prescribed stretch. Freestanding gel or polymer strip platforms have been designed to study patterned or biologically manipulated cardiomyocyte force generation.[82,83,84,85] Though early cardiomyocyte culture work focused on larger and more robust rat cardiomyocytes, transgenic mouse models of human arrhythmia phenotypes have motivated a shift to murine cell culture.[86,87] Non-mammalian models of human cardiac disease are also employed to study small numbers of cardiomyocytes under near-native mechanoelectric conditions.[88,89]

Working with neonatal cardiomyocytes, which are capable of forming mechanoelectric junctions in culture, geometrical cues presenting extracellular matrix protein have been found to guide cells into anisotropic and aligned morphology similar to that of developing myocardium.[90,91,92,93,94,95] Stretch devices have been designed which give options for studying micropatterned cardiomyocytes under physiological biaxial loading conditions.[51,96,97,98] When combined with optical methods for mapping changes in membrane potential, these techniques permit precise measurement with the capability to observe changes

in conduction (**Chapter 2** and **Chapter 3**) across aligned, uniformly and precisely stretched, multi-cellular preparations.[99] The length scale of the micropatterned cell culture permits study of arrhythmogenic mechanisms, including those associated with proarrhythmic substrate such as reentrant spiral waves (**Chapter 4**). These experimental setups allow for direct evaluation of mechanoelectric mechanisms at the multi-cellular level, giving insight into cell-level function and its role in overall cardiac MEF.

Engineered Cardiac Tissue

Engineered cardiac tissue (ECT) is a relatively new and emerging technology that can be used to study both the mechanical and electrical properties of the myocardium at the tissue scale. This method allows for the study of neonatal cardiomyocytes at the tissue scale, which was previously not feasible in intact preparations such as trabeculae or papillary muscles, due to the small size of neonatal hearts. ECTs initially utilized cardiomyocytes from embryonic chick hearts[100,101] and neonatal rat hearts.[90] Recently, the source of cardiomyocytes was expanded to include neonatal mouse hearts, which allows access to the multitude of gene-targeted mouse models of heart disease.[102] (Such genetic tools are utilized in **Chapter 3** and **Chapter 4,** in a micropatterned preparation). These preparations have been shown to propagate electrical impulse and produce calcium transients that are very representative of what is measured in traditional intact and whole heart preparations.[90,103] However, there are some concerns with the extracellular matrix structure, cell architecture, and cell-cell junctions that need to be addressed in these engineered tissues.

Ventricular Slice and Wedge Preparations

Other preparations that are used to study the myocardium at the tissue level are the ventricular slice and wedge. Ventricular wedge preparations have provided a wealth of knowledge regarding electrophysiology and arrythmogenesis, and have been shown to be a valid preclinical model.[104] These preparations keep the entire ventricular wall intact, which allows for determination of transmural electrophysiological heterogeneities that is not possible in many other preparations.[105] Studies were originally performed using canine ventricles, but have more recently been expanded to include human tissue.[76,106] Ventricular slice preparations have also been performed using human tissue, and consist of a very thin slice of tissue that is suitable for multi-cellular studies. Slice preparations provide stable electrical activity and have shown conduction velocities similar to that of the whole heart.[76] While this novel and highly promising approach provides an ideal framework for studying electrophysiology, using both optical and electrical methods, it has not yet been used for investigating mechanics or electromechanics, though this should be feasible.

Conclusions

The sequence of electrical activation in the whole heart has been shown to give rise to a relatively uniform contraction wave-front in the normal heart. This uniform contraction can be disrupted due to conduction disturbances such as localized blocks in the cardiac conduction system or aberrant effects of MEF, ultimately leading to dyssynchronous activation and contraction. It is known that dyssynchronous activation alters the electromechanics of the heart, but the mechanisms involved in this alteration are not completely understood. At the level of the single cell, ECC has been studied as a means to give insight to the electromechanics taking place at the whole heart scale, and MEF has been investigated in the context of component ion channels response to cell membrane tension. At this point in time, it

is fairly well understood how electrical excitation gives rise to mechanical contraction via calcium induced calcium release. However, studies at the cellular level lack the important cell-cell and cell-ECM mechanoelectrical interactions that are present in intact tissue. The lack of the ability to simulate dyssynchrony to study how it alters ECC, and the ability to apply precise mechanical loads to cell populations in order to understand MEF hinders progress toward identifying cell-scale mechanisms for organ-scale phenomena. Engineered cardiac tissue and ventricular wedge preparations are extremely useful for studying the electrophysiology of the myocardium, but require the ability to reliably study the mechanics to draw insight into MEF. Multi-cellular preparations with capability for biaxial stretch, such as described in **Chapter 2**, can provide this level of precision and show promise in identifying mechanisms of MEF, as demonstrated in **Chapter 3** and **Chapter 4**. These approaches to measuring cardiac mechanoelectric feedback will help bridge the gap in knowledge between what is well known at the cellular level, and how this information can be translated to the whole heart.

Acknowledgements

The content of Chapter 1 is almost identical to sections of a manuscript scheduled for publication in the *Journal of Biomechanical Engineering*, a publication of the American Society of Mechanical Engineers (ASME), with minor revisions and formatting changes for this dissertation. The authors and title of the submitted manuscript are as follows: Pfeiffer, E.R.,* Tangney, J.R.,* J.H. Omens, A.D. McCulloch, 2014. Biomechanics of cardiac electromechanical coupling and mechanoelectric feedback. Journal of Biomechanical Engineering.

References

[1] Prinzen FW, Peschar M. Relation between the pacing induced sequence of activation and left ventricular pump function in animals. *Pacing Clin. Electrophysiol.* 2002;25(4 Pt 1):484–98.

[2] Quinn TA, Bayliss RA, Kohl P. Mechano-electric feedback in the heart: effects on heart rate and rhythm. In: Tripathi ON, Ravens U, Sanguinetti MC, eds. *Heart Rate and Rhythm*. Berlin, Heidelberg: Springer Berlin Heidelberg; 2011:133–151.

[3] Leclercq C, Kass DA. Retiming the failing heart: principles and current clinical status of cardiac resynchronization. *J. Am. Coll. Cardiol.* 2002;39(2):194–201.

[4] Braunwald E. Research Advances in Heart Failure: A Compendium. *Circ. Res.* 2013;113(6):633–45.

[5] Coronel R, Wilders R, Verkerk AO, Wiegerinck RF, Benoist D, Bernus O. Electrophysiological changes in heart failure and their implications for arrhythmogenesis. *Biochim. Biophys. Acta*. 2013;1832(12):2432–41.

[6] Maron BJ, Doerer JJ, Haas TS, Estes NAM, Link MS. Historical observation on commotio cordis. *Hear. Rhythm*. 2006;3(5):605–606.

[7] Kohl P, Hunter P, Noble D. Stretch-induced changes in heart rate and rhythm: clinical observations, experiments and mathematical models. *Prog. Biophys. Mol. Biol.* 1999;71:91–138.

[8] Maron BJ, Haas TS, Ahluwalia A, Garberich RF, Estes NAM, Link MS. Increasing survival rate from commotio cordis. *Hear. Rhythm*. 2013;10(2):219–23.

[9] Madias C, Maron BJ, Alsheikh-ali AA, Estes NAM, Link MS. Commotio Cordis. *Indian Pacing Electrophysiol. J.* 2007;7(4):235–245.

[10] Trayanova N a, Constantino J, Gurev V. Models of stretch-activated ventricular arrhythmias. *J. Electrocardiol.* 2010;43(6):479–85.

[11] Hansen DE, Craig CS, Hondeghem LM. Stretch-induced arrhythmias in the isolated canine ventricle. Evidence for the importance of mechanoelectrical feedback. *Circulation*. 1990;81(3):1094–1105.

[12] Wang Z, Taylor LK, Denney WD, Hansen DE. Initiation of ventricular extrasystoles by myocardial stretch in chronically dilated and failing canine left ventricle. *Circulation*. 1994;90(4):2022–2031.

[13] Berdowski J, Tijssen JGP, Koster RW. Chest compressions cause recurrence of ventricular fibrillation after the first successful conversion by defibrillation in out-of-hospital cardiac arrest. *Circ. Arrhythmia Electrophysiol.* 2010;3(1):72–8.

[14] Janse MJ, Coronel R, Wilms-Schopman FJ., de Groot JR. Mechanical effects on arrhythmogenesis: from pipette to patient. *Prog. Biophys. Mol. Biol.* 2003;82(1-3):187–195.

[15] Pellis T, Kette F, Lovisa D, et al. Utility of pre-cordial thump for treatment of out of hospital cardiac arrest: a prospective study. *Resuscitation*. 2009;80(1):17–23.

[16] Pellis T, Kohl P. Extracorporeal cardiac mechanical stimulation: precordial thump and precordial percussion. *Br. Med. Bull.* 2010;93:161–77.

[17] Bainbridge FA. The influence of venous filling upon the rate of the heart. *J. Physiol.* 1915;50(2):65–84.

[18] Crystal GJ, Salem MR. The Bainbridge and the "reverse" Bainbridge reflexes: history, physiology, and clinical relevance. *Anesth. Analg.* 2012;114(3):520–32.

[19] Cui J, Gao Z, Blaha C a, Herr MD, Mast JL, Sinoway LI. Distension of central great vein decreases sympathetic outflow in humans. *Am. J. Physiol. - Hear. Circ. Physiol.* 2013;305(3):H378–85.

[20] Lab MJ. Contraction-excitation feedback in myocardium. Physiological basis and clinical relevance. *Circ. Res.* 1982;50(6):757–766.

[21] Marrus SB, Nerbonne JM. Mechanisms linking short- and long-term electrical remodeling in the heart … is it a stretch? *Channels*. 2008;2(2):117–124.

[22] Eckardt L, Kirchhof P, Monnig G, Breithardt G, Borggrefe M, Haverkamp W. Modification of stretch ¬induced shortening of repolarization by streptomycin in the isolated rabbit heart. *J. Cardiovasc. Pharmacol.* 2000;36(6):1–17.

[23] Franz MR, Bode F. Mechano-electrical feedback underlying arrhythmias: the atrial fibrillation case. *Prog. Biophys. Mol. Biol.* 2003;82(1-3):163–174.

[24] Kiseleva I, Kamkin A, Wagner K-D, et al. Mechanoelectric feedback after left ventricular infarction in rats. *Cardiovasc. Res.* 2000;45(2):370–8.

[25] McNary TG, Sohn K, Taccardi B, Sachse FB. Experimental and computational studies of strain-conduction velocity relationships in cardiac tissue. *Prog. Biophys. Mol. Biol.* 2008;97(2-3):383–400.

[26] Sung D, Mills RW, Schettler J, Narayan SM, Omens JH, McCulloch AD. Ventricular filling slows epicardial conduction and increases action potential duration in an optical mapping study of the isolated rabbit heart. *J. Cardiovasc. Electrophysiol.* 2003;14(7):739–749.

[27] Mills RW, Narayan SM, McCulloch AD. Mechanisms of conduction slowing during myocardial stretch by ventricular volume loading in the rabbit. *Am. J. Physiol. - Hear. Circ. Physiol.* 2008;295(3):H1270–H1278.

[28] Satoh T, Zipes DP. Unequal atrial stretch in dogs increases dispersion of refractoriness conducive to developing atrial fibrillation. *J. Cardiovasc. Electrophysiol.* 1996;7(9):833–42.

[29] Mills RW, Wright AT, Narayan SM, McCulloch AD. The effects of wall stretch on ventricular conduction and refractoriness in the whole heart. In: Kohl P, Sachs F, Franz MR, eds. *Cardiac Mechano-Electric Coupling and Arrhythmias*. 2nd ed. Oxford: Oxford University Press; 2011:180–186.

[30] Bett GC., Sachse FB. Cardiac mechanosensitivity and stretch-activated ion channels. *Trends Cardiovasc. Med.* 1997;7(1):4–8.

[31] Bowman CL, Gottlieb P a, Suchyna TM, Murphy YK, Sachs F. Mechanosensitive ion channels and the peptide inhibitor GsMTx-4: history, properties, mechanisms and pharmacology. *Toxicon*. 2007;49(2):249–70.

[32] Dyachenko V, Husse B, Rueckschloss U, Isenberg G. Mechanical deformation of ventricular myocytes modulates both TRPC6 and Kir2.3 channels. *Cell Calcium*. 2009;45(1):38–54.

[33] Hu H, Sachs F. Stretch-activated ion channels in the heart. *J. Mol. Cell. Cardiol.* 1997;29:1511–1523.

[34] Spassova M a, Hewavitharana T, Xu W, Soboloff J, Gill DL. A common mechanism underlies stretch activation and receptor activation of TRPC6 channels. *Proc. Natl. Acad. Sci. U. S. A.* 2006;103(44):16586–91.

[35] Suchyna TM, Johnson JH, Hamer K, et al. Identification of a peptide toxin from Grammostola spatulata spider venom that blocks cation-selective stretch-activated channels. *J. Gen. Physiol.* 2000;115(5):583–98.

[36] Eder P, Molkentin JD. TRPC channels as effectors of cardiac hypertrophy. *Circ. Res.* 2011;108(2):265–72.

[37] Friedrich O, Wagner S, Battle AR, Schürmann S, Martinac B. Mechano-regulation of the beating heart at the cellular level - Mechanosensitive channels in normal and diseased heart. *Prog. Biophys. Mol. Biol.* 2012;110(2-3):226–38.

[38] Quinn TA, Kohl P. Mechano-sensitivity of cardiac pacemaker function: pathophysiological relevance, experimental implications, and conceptual integration with other mechanisms of rhythmicity. *Prog. Biophys. Mol. Biol.* 2012;110(2-3):257–68.

[39] Healy SN, McCulloch AD. An ionic model of stretch-activated and stretch-modulated currents in rabbit ventricular myocytes. *Europace*. 2005;7:S128–34.

[40] Kong C-R, Bursac N, Tung L. Mechanoelectrical excitation by fluid jets in monolayers of cultured cardiac myocytes. *J. Appl. Physiol.* 2005;98(6):2328–36.

[41] Weise LD, Panfilov A V. A discrete electromechanical model for human cardiac tissue: effects of stretch-activated currents and stretch conditions on restitution properties and spiral wave dynamics. Garcia-Ojalvo J, ed. *PLoS One*. 2013;8(3):e59317.

[42] Clapham DE, Shrier A, DeHaan RL. Junctional resistance and action potential delay between embryonic heart cell aggregates. *J. Gen. Physiol.* 1980;75(6):633–54.

[43] Elfgang C, Eckert R, Lichtenberg-Fraté H, et al. Specific permeability and selective formation of gap junction channels in connexin-transfected HeLa cells. *J. Cell Biol.* 1995;129(3):805–17.

[44] Gourdie RG. A map of the heart: gap junctions, connexin diversity and retroviral studies of conduction myocyte lineage. *Clin. Sci.* 1995;88:257–262.

[45] Severs NJ, Bruce AF, Dupont E, Rothery S. Remodelling of gap junctions and connexin expression in diseased myocardium. *Cardiovasc. Res.* 2008;80(1):9–19.

[46] Weingart R. Electrical properties of the nexal membrane studied in rat ventricular cell pairs. *J. Physiol.* 1986;370:267–284.

[47] Fontes MSC, van Veen T a B, de Bakker JMT, van Rijen HVM. Functional consequences of abnormal Cx43 expression in the heart. *Biochim. Biophys. Acta*. 2011;1818(8):2020–9.

[48] Saffitz JE, Laing JG, Yamada K a. Connexin expression and turnover: implications for cardiac excitability. *Circ. Res.* 2000;86:723–728.

[49] Saffitz JE. Dependence of electrical coupling on mechanical coupling in cardiac myocytes: insights gained from cardiomyopathies caused by defects in cell-cell connections. *Ann. N. Y. Acad. Sci.* 2005;1047:336–44.

[50] Cherian PP, Siller-Jackson AJ, Gu S, et al. Mechanical strain opens connexin 43 hemichannels in osteocytes: a novel mechanism for the release of prostaglandin. *Mol. Biol. Cell*. 2005;16(7):3100–6.

[51] Gopalan SM, Flaim C, Bhatia SN, et al. Anisotropic stretch-induced hypertrophy in neonatal ventricular myocytes micropatterned on deformable elastomers. *Biotechnol. Bioeng.* 2003;81(5):578–87.

[52] Zhuang J, Yamada K a, Saffitz JE, Kléber AG. Pulsatile stretch remodels cell-to-cell communication in cultured myocytes. *Circ. Res.* 2000;87(4):316–22.

[53] Kontogeorgis A, Kaba R a, Kang E, et al. Short-term pacing in the mouse alters cardiac expression of connexin43. *BioMed Cent. Physiol.* 2008;8:8.

[54] Poelzing S, Rosenbaum DS. Altered connexin43 expression produces arrhythmia substrate in heart failure. *Am. J. Physiol. - Hear. Circ. Physiol.* 2004;287(4):H1762–70.

[55] Rhett JM, Veeraraghavan R, Poelzing S, Gourdie RG. The perinexus: sign-post on the path to a new model of cardiac conduction? *Trends Cardiovasc. Med.* 2013;23(6):222–228.

[56] Hand PE, Peskin CS. Homogenization of an electrophysiological model for a strand of cardiac myocytes with gap-junctional and electric-field coupling. *Bull. Math. Biol.* 2010;72(6):1408–24.

[57] Lin J, Keener JP. Ephaptic coupling in cardiac myocytes. *IEEE Trans. Biomed. Eng.* 2013;60(2):576–82.

[58] Roberts SF, Stinstra JG, Henriquez CS. Effect of nonuniform interstitial space properties on impulse propagation: a discrete multidomain model. *Biophys. J.* 2008;95(8):3724–37.

[59] Kohl P, Cooper PJ, Holloway H. Effects of acute ventricular volume manipulation on in situ cardiomyocyte cell membrane configuration. *Prog. Biophys. Mol. Biol.* 2003;82(1-3):221–227.

[60] McNary TG, Spitzer KW, Holloway H, Bridge JHB, Kohl P, Sachse FB. Mechanical modulation of the transverse tubular system of ventricular cardiomyocytes. *Prog. Biophys. Mol. Biol.* 2012;110(2-3):218–225.

[61] Suchyna TM, Tape SE, Koeppe RE, Andersen OS, Sachs F, Gottlieb PA. Bilayer-dependent inhibition of mechanosensitive channels by neuroactive peptide enantiomers. *Nature*. 2004;430(6996):235–240.

[62] Maleckar MM, Greenstein JL, Giles WR, Trayanova NA. Electrotonic coupling between human atrial myocytes and fibroblasts alters myocyte excitability and repolarization. *Biophys. J.* 2009;97(8):2179–90.

[63] Miragoli M, Gaudesius G, Rohr S. Electrotonic modulation of cardiac impulse conduction by myofibroblasts. *Circ. Res.* 2006;98(6):801–10.

[64] Rook M, Jongsma H, Jonge B. Single channel currents of homo- and heterologous gap junctions between cardiac fibroblasts and myocytes. *Pflügers Arch. Eur. J. Physiol.* 1989;414(1):95–98.

[65] Rudy Y. Electrotonic cell-cell interactions in cardiac tissue: effects on action potential propagation and repolarization. *Ann. N. Y. Acad. Sci.* 2005;1047:308–13.

[66] Kohl P, Kamkin A, Kiseleva IS, Streubel T. Mechanosensitive cells in the atrium of frog heart. *Exp. Physiol.* 1992;77(1):213–6.

[67] Kohl P, Kamkin A, Kiseleva IS, Noble D. Mechanosensitive fibroblasts in the sino-atrial node region of rat heart: interaction with cardiomyocytes and possible role. *Exp. Physiol.* 1994;79(6):943–56.

[68] Haraguchi Y, Shimizu T, Yamato M, Okano T. Electrical interaction between cardiomyocyte sheets separated by non-cardiomyocyte sheets in heterogeneous tissues. *Tissue Eng.* 2010;4:291–299.

[69] Rohr S. Myofibroblasts in diseased hearts: new players in cardiac arrhythmias? *Hear. Rhythm*. 2009;6(6):848–56.

[70] Vasquez C, Benamer N, Morley GE. The cardiac fibroblast: functional and electrophysiological considerations in healthy and diseased hearts. *J. Cardiovasc. Pharmacol.* 2011;57(4):380–388.

[71] Thompson SA, Copeland CR, Reich DH, Tung L. Mechanical coupling between myofibroblasts and cardiomyocytes slows electric conduction in fibrotic cell monolayers. *Circulation*. 2011;123(19):2083–93.

[72] Suchyna TM, Sachs F. Mechanosensitive channel properties and membrane mechanics in mouse dystrophic myotubes. *J. Physiol.* 2007;581(1):369–87.

[73] Sokabe M, Sachs F, Jing ZQ. Quantitative video microscopy of patch clamped membranes stress, strain, capacitance, and stretch channel activation. *Biophys. J.* 1991;59(3):722–8.

[74] Morris C, Homann U. Cell surface area regulation and membrane tension. *J. Membr. Biol.* 2001;179:79–102.

[75] Isenberg G, Kondratev D, Dyachenko V, Kazanski V, Gallitelli. MF. Isolated cardiomyocytes: mechanosensitivity of action potential, membrane current and ion concentration. In: Kamkin A, Kiseleva I, eds. *Mechanosensitivity in Cells and Tissues*. Moscow: Academia Publishing House Ltd.; 2005.

[76] Camelliti P, Al-Saud SA, Smolenski RT, et al. Adult human heart slices are a multicellular system suitable for electrophysiological and pharmacological studies. *J. Mol. Cell. Cardiol.* 2011;51(3):390–8.

[77] Seo K, Inagaki M, Nishimura S, et al. Structural heterogeneity in the ventricular wall plays a significant role in the initiation of stretch-induced arrhythmias in perfused rabbit right ventricular tissues and whole heart preparations. *Circ. Res.* 2010;106(1):176–84.

[78] de Boer TP, Camelliti P, Ravens U, Kohl P. Myocardial tissue slices: organotypic pseudo-2D models for cardiac research & development. *Future Cardiol.* 2009;5(5):425–430.

[79] Engler AJ, Carag-Krieger C, Johnson CP, et al. Embryonic cardiomyocytes beat best on a matrix with heart-like elasticity: scar-like rigidity inhibits beating. *J. Cell Sci.* 2008;121(Pt 22):3794–802.

[80] Jacot JG, McCulloch AD, Omens JH. Substrate stiffness affects the functional maturation of neonatal rat ventricular myocytes. *Biophys. J.* 2008;95(7):3479–87.

[81] Yeung T, Georges PC, Flanagan LA, et al. Effects of substrate stiffness on cell morphology, cytoskeletal structure, and adhesion. *Cell Motil. Cytoskeleton*. 2005;60(1):24–34.

[82] Alford PW, Feinberg AW, Sheehy SP, Parker KK. Biohybrid thin films for measuring contractility in engineered cardiovascular muscle. *Biomaterials*. 2010;31(13):3613–21.

[83] Aubin H, Nichol JW, Hutson CB, et al. Directed 3D cell alignment and elongation in microengineered hydrogels. *Biomaterials*. 2010;31(27):6941–6951.

[84] Sarig U, Machluf M. Engineering cell platforms for myocardial regeneration. *Expert Opin. Biol. Ther.* 2011;11(8):1055–77.

[85] Nawroth JC, Lee H, Feinberg AW, et al. A tissue-engineered jellyfish with biomimetic propulsion. *Nat. Biotechnol.* 2012;30:792–797.

[86] Davis J, Westfall M V, Townsend D, et al. Designing Heart Performance by Gene Transfer. *Physiol. Rev.* 2008;88:1567–1651.

[87] Houser SR, Margulies KB, Murphy AM, et al. Animal models of heart failure: a scientific statement from the American Heart Association. *Circ. Res.* 2012;111:131–150.

[88] Arrenberg AB, Stainier DY, Baier H, Huisken J. Optogenetic control of cardiac function. *Science (80).* 2010;330(6006):971–4.

[89] Kaushik G, Fuhrmann A, Cammarato A, Engler AJ. In situ mechanical analysis of myofibrillar perturbation and aging on soft, bilayered drosophila myocardium. *Biophys. J.* 2011;101(11):2629–2637.

[90] Rohr S, Scholly D, Kleber AG. Patterned growth of neonatal rat heart cells in culture. Morphological and electrophysiological characterization. *Circ. Res.* 1991;68(114-130).

[91] Bursac N, Parker KK, Iravanian S, Tung L. Cardiomyocyte cultures with controlled macroscopic anisotropy: a model for functional electrophysiological studies of cardiac muscle. *Circ. Res.* 2002;91(12):e45e–54.

[92] Camelliti P, McCulloch AD, Kohl P. Microstructured cocultures of cardiac myocytes and fibroblasts: a two-dimensional in vitro model of cardiac tissue. *Microsc. Microanal.* 2005;11(3):249–59.

[93] Costa KD, Lee EJ, Holmes JW. Creating alignment and anisotropy in engineered heart tissue: role of boundary conditions in a model three-dimensional culture system. *Tissue Eng.* 2003;9(4):567–77.

[94] Kuo P-L, Lee H, Bray M-A, et al. Myocyte shape regulates lateral registry of sarcomeres and contractility. *Am. J. Pathol.* 2012;181(6):2030–7.

[95] McDevitt T, Angello J, Whitney M, et al. In vitro generation of differentiated cardiac myofibers on micropatterned laminin surfaces. *J. Biomed. Mater. Res.* 2002;60(3):472–9.

[96] Barbee KA, Macarak EJ, Thibault LE. Strain measurements in cultured vascular smooth muscle cells subjected to mechanical deformation. *Ann. Biomed. Eng.* 1994;22(1):14–22.

[97] Lee AA, Delhaas T, McCulloch AD, Villarreal FJ. Differential responses of adult cardiac fibroblasts to in vitro biaxial strain patterns. *J. Mol. Cell. Cardiol.* 1999;31(10):1833–43.

[98] Camelliti P, Gallagher JO, Kohl P, McCulloch AD. Micropatterned cell cultures on elastic membranes as an in vitro model of myocardium. *Nat. Protoc.* 2006;1(3):1379–91.

[99] Zhang Y, Sekar RB, McCulloch AD, Tung L. Cell cultures as models of cardiac mechanoelectric feedback. *Prog. Biophys. Mol. Biol.* 2008;97(2-3):367–382.

[100] Eschenhagen T, Fink C, Remmers U, et al. Three-dimensional cardiomyocytes muscle model reconstitution in a collagen system of embryonic matrix : a new heart. *FASEB J.* 1997;11:683–694.

[101] Asnes CF, Marquez JP, Elson EL, Wakatsuki T. Reconstitution of the Frank-Starling mechanism in engineered heart tissues. *Biophys. J.* 2006;91(5):1800–10.

[102] de Lange WJ, Hegge LF, Grimes a C, et al. Neonatal mouse-derived engineered cardiac tissue: a novel model system for studying genetic heart disease. *Circ. Res.* 2011;109:8–19.

[103] Ralphe JC, de Lange WJ. 3D engineered cardiac tissue models of human heart disease: learning more from our mice. *Trends Cardiovasc. Med.* 2013;23(2):27–32.

[104] Liu T, Brown BS, Wu Y, Antzelevitch C, Kowey PR, Yan G-X. Blinded validation of the isolated arterially perfused rabbit ventricular wedge in preclinical assessment of drug-induced proarrhythmias. *Hear. Rhythm*. 2006;3(8):948–56.

[105] Di Diego JM, Sicouri S, Myles RC, Burton FL, Smith GL, Antzelevitch C. Optical and electrical recordings from isolated coronary-perfused ventricular wedge preparations. *J. Mol. Cell. Cardiol.* 2013;54:53–64.

[106] Glukhov A V, Fedorov V V, Lou Q, et al. Transmural dispersion of repolarization in failing and nonfailing human ventricle. *Circ. Res.* 2010;106(5):981–91.

Chapter 2

Stretch-Dependent Electrophysiology in Multicellular Preparations

Introduction

While phenomena of MEF in mechanically-induced dyssynchrony and arrhythmia have been observed, the mechanisms and implications for cardiac electrophysiology in normal and diseased function are incompletely understood.[1] In fact, published reports of the nature of the effect of stretch on conduction in the whole heart and muscle preparations disagree on whether stretch results in a conduction velocity increase or decrease.[2] Among these, studies in intact rabbit hearts indicate conduction slowing with ventricular inflation, a proarrhythmic effect which leaves not yet excited areas vulnerable to reentry and aberrant excitation.[3,4] Whether speeding or slowing, changes in conduction induced by a heterogeneous strain field are likely to promote dyssynchronous spread of activation, leading to inefficient pumping and heart failure.[5] Arrhythmogenic MEF effects in the heart have been attributed to stretch modulation of ion channels, cell-cell coupling, or changes in the resistive and capacitive electrical properties of the myocardium, however experimental models which can probe the role of intra- and inter-cellular mechanisms at a tissue spatial scale have not been widely implemented in approaching these questions.[6]

Physiological Stretch Magnitude

A range of diastolic stretch magnitudes have been reported in cardiac tissue *in vivo*. The typical model for these studies is the isolated and arrested dog heart, inflated to physiological left ventricular end diastolic pressures (often using an inserted balloon). Strain anisotropy was demonstrated by McCulloch et al., who found major and minor axes of midanterior epicardial extension of 13.9±1.2% and 7.2±3.2%, respectively, at 20mmHg pressure.[7] A follow-up report indicated that the direction of greatest passive stretch

corresponded with the epicardial fiber orientation, and that stretch generally increased from base to apex, exceeding 20-25% between the midventricle and apex.[8] Subsequent studies reported that alignment of fibers and maximum strain varied transmurally, with greatest strain shifting away from the fiber direction toward the cross-fiber direction in planes nearer the endocardium, yet with fibers experiencing fiber-parallel strain increasing from approximately 5% to 20% from epicardium to endocardium, and with fiber-perpendicular strain varying between 5% and 10% transmurally.[9] Strain anisotropy in passively inflated rat hearts has been observed to be consistent with dog, with maximum strain near 20% at 25-30 mmHg pressure loading.[10,11] While some species differences in myocardium constitutive properties and stresses were observed,[10] these results suggest that end diastole fiber and cross-fiber strains are relatively similar between large and small mammals. Healthy stretch can be expected to vary regionally and directionally, but average on the order of 10%, while regional and particularly disease perturbed stretch can exceed these levels.

Tissue-Scale Multicellular Preparations

Discrepancies in stretch effects on conduction measured *in situ* may be partially attributed to the geometrical warping of tissue and interstitial fluid redistribution that occurs with loading in these preparations. In isolated heart experiments, ventricular wall volume changes including edema can be limited by minimizing the duration of perfusion,[10] however interstitial fluid effects are difficult to fully assess and control. Concerns regarding nonhomogeneous changes in the interstitium are eliminated in a cardiomyocyte monolayer culture model system, which may be particularly useful in the study of cardiac MEF,[12] especially when designed at the spatial scale of conduction and arrhythmia phenomena observed in tissue.[13]

Complications regarding tissue geometry reorientation with respect to the stretch and observation planes can be minimized within cell culture models through the use of micropatterned elastomeric substrates.[14] In micropatterned monolayer preparations, each cardiomyocyte may only activate its immediate neighbors, thus changes in conduction path due to geometrical warping of tissue during stretch are precluded.[15] Micropatterned substrates have been used to induce cardiomyocyte elongation, alignment and coupling,[16,17] and have been coupled with substrate stretch mainly to study hypertrophic signaling[18,19,20] though potential for use in measuring MEF has been demonstrated.[13]

Stretch Application

The applied strain field is an important consideration in the design of MEF experiments. Biaxial stretch of micropatterned cultures provides a loading paradigm which is more representative of myocardial wall stress than is uniaxial stretch, mimicking the deformations applied to a cell during cardiac volume loading.[21,22] Unlike stretch along one cell axis, in which the two unconstrained dimensions experience compressive stresses, or osmotic swelling, in which the cell expands isotropically in three dimensions, biaxial stretch mimics the unique deformations applied to the costameres, membrane ultrastructure, cell-cell junctions and sarcomeres of the myocyte during cardiac loading.[21] Previous work has shown that biaxial anisotropy is important in mechanotransduction of cardiac hypertrophy.[18,20]

Methods

A customized platform was used to study MEF in a multicellular cardiomyocyte preparation, at spatial scales reflecting tissue-scale electrophysiological phenomena. In this preparation, cardiomyocytes are cultured on a micropatterned elastomeric substrate mounted in a biaxial stretch device and studied using optical mapping of cardiomyocyte membrane potential.

Microfabricated Substrate

Micropatterned polydimethylsiloxane (PDMS) elastomeric cell culture substrates were manufactured following a three-step process: (1) photolithographic patterning of silicon wafer molds, (2) PDMS molding and polymerization, (3) extracellular matrix (ECM) adsorption. This technique results in a microgrooved surface with channels 10 μm wide, 10 μm apart and 5 μm deep, which provide "2.5 dimensional" structural and biochemical cues that result in optimal facilitation of cardiomyocyte elongation, alignment, and coupling when compared with traditional flat tissue culture substrates.[14,19]

Photolithographic patterning was used to transfer rectangular patterns from a titanium mask into three-dimensional structures on silicon wafers. The wafers were coated with a thin layer of SU-8 2005 negative photoresist (MicroChem), which when exposed to UV light, cross-links to permanently adhere to the wafer. Following exposure, the photoresist was "developed", or dissolved away from the exposed pattern, leaving rectangular photoresist pillars. Following hardening and anti-adhesive silane treatment, the wafers bearing photoresist structures were used to mold PDMS. Sylgard 186 elastomer base and curing agent were mixed at a standard (10:1) ratio, molded via spin-coating onto the patterned wafers. The polymer was cured for 30 minutes at 70°C, and overnight at room temperature prior to removal from the

molds and fitting to stretch devices. Laminin, a basal membrane ECM protein and preferential binding substrate for differentiated cardiomyocytes,[23] was adsorbed onto the PDMS prior to cell culture using a 10 minute UV exposure. Laminin plays a physiological role in expression of gap junction proteins,[24] localization of caveolin-3 which induces membrane curvature at caveolae and t-tubules,[25] and scaffolding components of β-adrenergic[26] signaling pathways. Neonatal mouse ventricular myocytes (NMVMs) cultured on these substrates for 2-4 days demonstrated elongation, alignment, and mechanoelectric coupling with surrounding cells as seen in **Figure 2.1**.

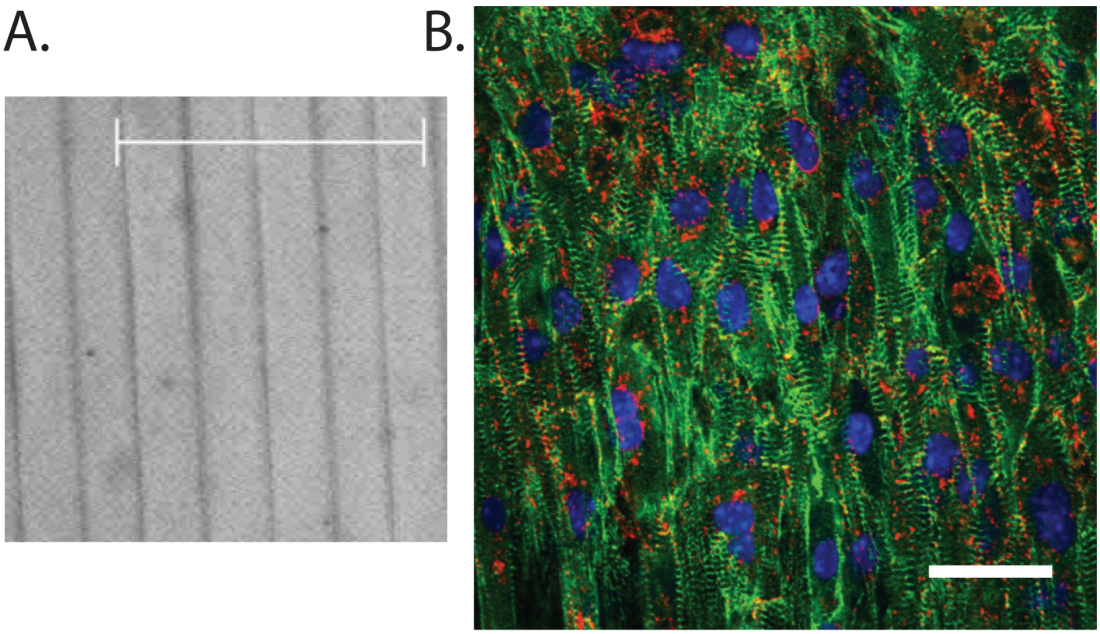

Figure 2.1: Micropatterned PDMS promotes elongation and alignment of cardiomyocytes. A) Image of micropatterned PDMS, scale 50 µm. B) Neonatal mouse ventricular myocytes, cultured on micropatterned PDMS for 3 days following isolation and immunofluorescently labeled. Green: sarcomeric α-actinin, red: connexin-43, blue: DAPI. Scale 30 µm. Adapted from *(In Preparation)* Pfeiffer, et al., 2014).

Optical Mapping

Optical mapping techniques for imaging cardiac electrophysiology were adapted for assessment of conduction in a two-dimensional culture. This method utilizes the high temporal and spatial resolution imaging of a CMOS camera (MiCAM Ultima-L) to capture rapid spectral shifts of a voltage-sensitive transmembrane fluorescent dye (di-8-ANEPPS), preventing obfuscation of conduction velocity measurements by so-called 'zig-zag'[15] conduction paths between dispersed measurement electrodes, and avoiding potential interactions from measurement electrode. The culture area is maintained at 37 °C, to avoid any thermal artifacts in mechanical and electrical properties of the cardiomyocytes.[27] In this preparation, the electrical substrate studied is fixed in position relative to the camera throughout the loading conditions, and biaxially deformed along the plane perpendicular to the light path (**Fig. 2.2**). Recordings are taken prior to mechanical loading, following 5 minutes of sustained stretch, and again 5 minutes following the removal of load. Stretch application is performed at a rate near 20%.min^{-1}

Measures were taken to control electrophysiological artifacts of voltage-sensitive dye loading. Reactive oxygen species (ROS) generation is a known source of electrophysiological artifact arising from the excitation of voltage-sensitive small molecule fluorescent dyes as well as from tissue isolation from systemic ROS-scavenging systems, having the general effect of conduction slowing and repolarization heterogeneity with significant exposure to excitation light.[28] Antioxidants were added to the optical mapping dye and test solutions at physiological levels, a measure used with success in other applications to check the generation of ROS by voltage-sensitive dye.[29] These extended the time of light exposure allowable before phototoxic electrophysiological effects to double that necessary for a successful set of baseline, stretched, and unstretched experiments per culture. Solutions including antioxidants

were prepared from powder on the day of use, to avoid any decay of antioxidant activity in solution.

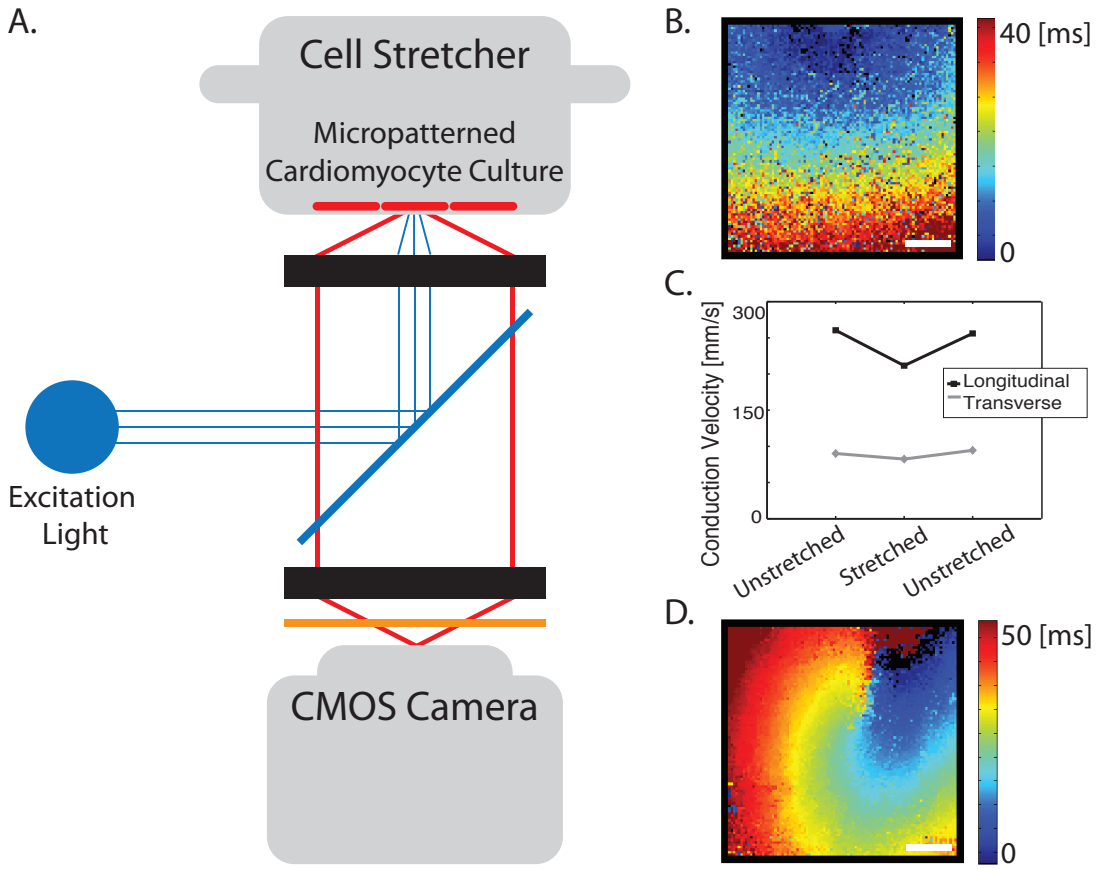

Figure 2.2: Combined apparatus for biaxial stretch of micropatterned neonatal cardiomyocytes and optical mapping of cell membrane potential permits study of conduction through multi-cellular preparations. A) Diagram of optical mapping and micropatterned stretch equipment; B) Representative map of electrical activation, spatial scale 2 mm; C) Example stretch experiment result, showing that conduction in the longitudinal and transverse directions of the micropatterned cell culture slows with biaxial stretch, scale 2 mm; D) example activation map in a transgenic mouse model of arrhythmia associated with mechanoelectric junctions, in collaboration with Dr. Farah Sheikh, UCSD. Figure is adapted from *(In Press)* Pfeiffer, et al. 2014 Journal of Biomechanical Engineering).[6]

Results

Stretch Range

Stretch experiments were conducted, with recordings taken at baseline, loaded, and following load removal, using a range of anisotropic biaxial stretch regimes. At baseline, the anisotropy ratio of conduction of these cultures was 3.5±0.3 (N=44). Each cell culture studied was subjected to only one loading level, ranging from 2.3×0.6% to 14×3.6%. At low levels of stretch, conduction velocity generally increased from before loading, while at larger levels of stretch, conduction slowed (**Fig. 2.3**). This trend was observed regardless of whether the maximum or minimum stretch direction was oriented parallel to the fiber direction (taken to be in line with the microgrooves). However, greater variation (notably, toward positive conduction velocity change with stretch) was observed in the conduction direction normal to the maximum stretch direction at mid-range stretches (**Table 2.1**).

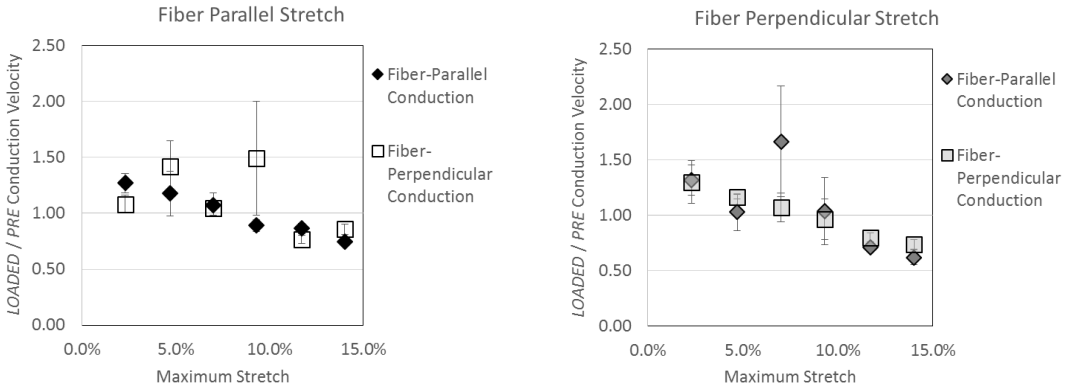

Figure 2.3: Conduction speeding and slowing with stretch depends more on stretch magnitude than on conduction or stretch direction.

Table 2.1: Ratio of loaded to initial conduction velocities of all groups measured.

Stretch			Conduction: *LOADED/BEFORE*			
Fiber-Parallel	Fiber-Perpendicular	N	Fiber-Parallel		Fiber-Perpendicular	
			mean	SEM	mean	SEM
14.0%	3.6%	8	0.75	0.04	0.86	0.05
11.7%	3.0%	3	0.86	0.05	0.77	0.04
9.3%	2.4%	2	0.89	0.05	1.49	0.51
7.0%	1.8%	4	1.08	0.10	1.05	0.07
4.7%	1.2%	2	1.18	0.20	1.42	0.23
2.3%	0.6%	7	1.27	0.09	1.08	0.08
3.6%	14.0%	4	0.62	0.07	0.74	0.04
3.0%	11.7%	3	0.71	0.03	0.80	0.04
2.4%	9.3%	2	1.03	0.30	0.96	0.18
1.8%	7.0%	4	1.66	0.50	1.07	0.13
1.2%	4.7%	2	1.03	0.17	1.17	0.02
0.6%	2.3%	3	1.32	0.14	1.30	0.19

Smallest Stretches

A one-way repeated measures ANOVA detected a significant difference between before loading (496±55 $mm.s^{-1}$), loaded (613±53 $mm.s^{-1}$), and after load was applied then removed (580±39 $mm.s^{-1}$) fiber-parallel conduction velocities under fiber-parallel 2.3×0.6% stretch (P=0.001, N=7), and a post-hoc multiple comparison test using Tukey procedures found a statistically significant increase in loaded from before loading (P=0.001), and between unloaded following loading *vs.* before loading (P=0.013), but not between loaded and following load application and removal (P=0.394) (**Fig. 2.4**). No significant differences were found between before loading, loading, and following load application and removal fiber-perpendicular conduction (P=0.486). The approximately 30% increase in conduction when the maximum direction of stretch was oriented fiber perpendicular was not detected to be significant in either fiber parallel or fiber perpendicular conduction (N=3, P=0.338, P=0.188 respectively).

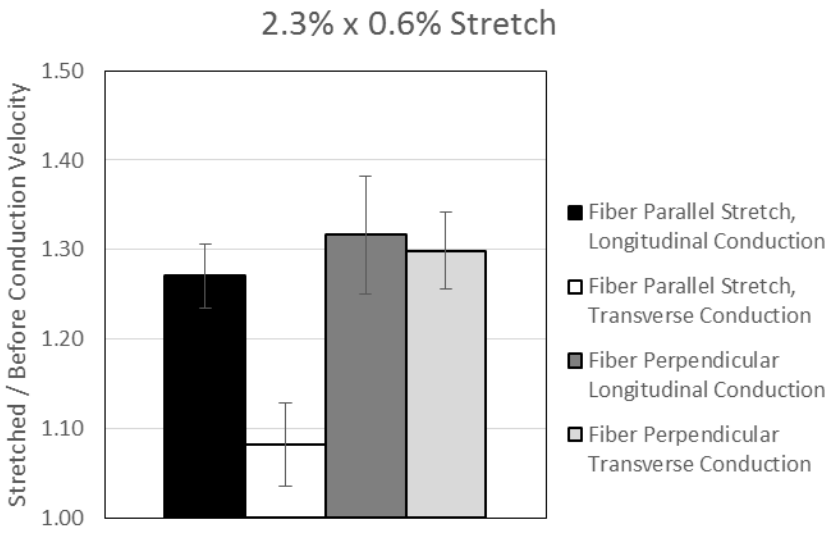

Figure 2.4: Conduction speeding is observed with small stretch. The increase in conduction velocity is significant only in fiber parallel conduction under fiber parallel stretch (P=0.001).

Largest Stretches

Conversely, conduction slowing was observed at larger stretches within the physiological diastolic range (**Fig. 2.5**). A significant difference was detected between before loading (325±30 $mm.s^{-1}$), loaded (248±33 $mm.s^{-1}$), and following load application and removal (294±34 $mm.s^{-1}$) fiber-parallel conduction velocities under fiber-parallel 14×3.6% stretch ($P<0.001$, $N=8$), and a post-hoc multiple comparison test using Tukey procedures found a statistically significant increase in loaded from baseline ($P<0.001$), between load application and removal and baseline ($P=0.04$), and between loaded and following load application and removal ($P=0.003$). Slowing in fiber-perpendicular conduction was not detected to be significant.

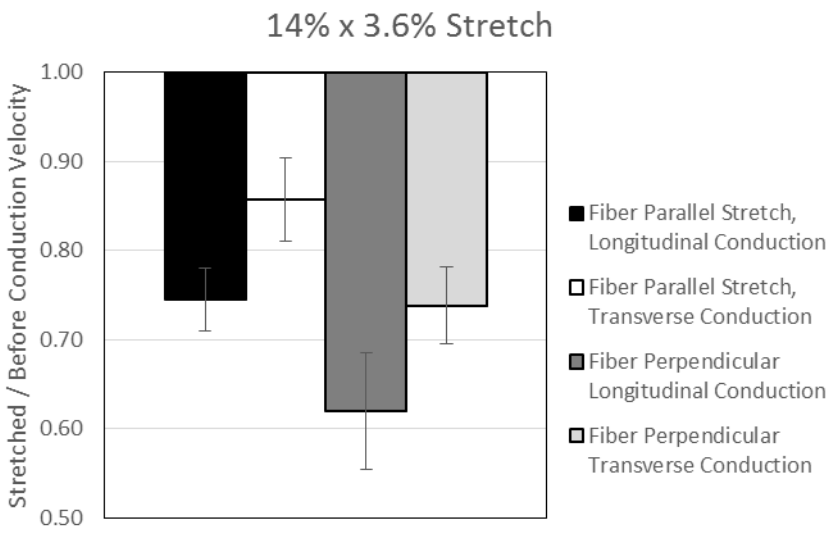

Figure 2.5: Conduction slowing is observed with large stretch. The decrease in conduction velocity was significant in fiber-parallel conduction under fiber-parallel stretch, and in both directions under fiber-perpendicular stretch.

In the case of fiber-perpendicular 14×3.6% stretch, a significant change in fiber-parallel conduction between treatments was detected (P=0.38, N=4). Fiber-parallel conduction slowed significantly from the unloaded state (409±83 $mm.s^{-1}$) to the loaded state (253±60 $mm.s^{-1}$) (P=0.045), and was not significantly different from before loading to after load had been applied then removed (272±117 $mm.s^{-1}$). A significant change in fiber-perpendicular conduction was also detected (P=0.016), where conduction slowed significantly from before loading (236±110 $mm.s^{-1}$) to loaded (181±92 $mm.s^{-1}$) (P=0.024), and remained significantly different from before loading at the unloaded condition following loading (182±105 $mm.s^{-1}$) (P=0.025).

Conclusions

Taken together, conduction responses over the ranges of stretch tested demonstrate a nominally linear shift from conduction speeding to conduction slowing between small (2.3×0.6%) and large (14×3.6%) stretch regimes, crossing "no change" at approximately 7-10% maximum stretch. This suggests the existence of at least two mechanisms of stretch-dependent conduction change, one resulting in conduction increase and possibly triggered only at small stretches, the other resulting in conduction decrease and perhaps more sensitive at larger stretches.

The conduction speeding response demonstrates a greater degree of anisotropy than the conduction slowing response. Though the conduction slowing response at 14×3.6% stretch was not fully isotropic (fiber-perpendicular conduction change under fiber-parallel stretch did not reach significance), 3 of the 4 measurements compared did. In conduction speeding at 2.3×0.6% stretch, 1 of the 4 cases was detected to be significant. This anisotropy of response suggests the mechanism for these small-stretch conduction increases could be linked to a molecular component structurally polarized within the cell, for example, gap junctions which are preferentially distributed at the ends of the long axis of cardiomyocytes.[30] In contrast, the more isotropic distribution of conduction slowing responses suggests a non-polarized cell mechanism, perhaps distributed uniformly over the cell surface, for example, caveolae. Where variations from the approximately linear trend exist, they are manifested as positive (speeding) variations in conduction along the minimum direction of stretch in mid-range stretch magnitudes, thus where the axis of conduction experiences a collinear stretch in the low stretch range seen to trigger stretch-parallel conduction speeding. This anisotropy further suggests an anisotropic mechanism for speeding.

Limitations of these observations include the variation in initial conduction velocities across experiments and the translation of results in multicellular preparation to organ-level physiology. In the 44 experiments described, fiber-parallel conduction ranged between 167-1213 $mm.s^{-1}$ (468±37 $mm.s^{-1}$) and fiber-perpendicular conduction ranged between 56-564 $mm.s^{-1}$ (166±15 $mm.s^{-1}$), with anisotropy ratios of conduction ranging between 1.1-9.4 (3.5±0.3). This variation is expected based on the timecourse of development of mechanoelectrical junctions in neonatal cells.[30] While changes in ratios of loaded to before loading conduction velocities appeared relatively consistent, the original variation in unloaded conduction velocities obscure the ability to test for the changes with stretch. While the inherent variation in baseline conduction is greater than that recorded in the intact heart, these observations of conduction slowing with diastolic levels of stretch are consistent with observations at the organ level. In acute, passive loading of intact rabbit ventricles to diastolic pressures, conduction was observed to slow by approximately 15% averaged across the epicardium.[3,4]

While stretch of the substrate and cell monolayer could increase the effective conduction velocity measured even if the time separating activation of two neighboring cells remains unchanged, this possible artifact acts at an order of magnitude below the conduction speeding we observed, and in opposition to the conduction slowing we observed. This system has the distinct advantage that no mechano-electric uncoupling agents or added physical constraints are required, as in the case with many whole heart studies. In those cases, uncoupling agents are administered or mechanical confinement is added to avoid motion artifacts of heartbeat during measurement, but have the potential to induce electrophysiological effects.[31] Artifacts of altered electrical resistance or capacitance due to movement of interstitial fluid are also eliminated in this system.

In summary, multicellular micropatterned preparations of NMVMs have been used successfully to demonstrate MEF due to biaxial stretch

Acknowledgements

Chapter 2 adapts a figure from the following manuscript scheduled for publication: Pfeiffer, E.R.,* Tangney, J.R.,* J.H. Omens, A.D. McCulloch, 2014. Biomechanics of cardiac electromechanical coupling and mechanoelectric feedback. Journal of Biomechanical Engineering. An image is also adapted from the Online Supplement of a manuscript in preparation for publication in *Circulation Research*. Besides this, the content of Chapter 2 is original. The author would like to thank Jennifer Stowe, Kyle Buchholz, Katie McNall, Justin Tan, Tammy Soo-Hoo and Tik-Chee (Jenny) Cheng for their assistance, as well as Adam Wright, Barbara Murienne, and Amy Hsieh for their technical legacies.

References

---

[1] Quinn TA, Bayliss RA, Kohl P. Mechano-electric feedback in the heart: effects on heart rate and rhythm. In: Tripathi ON, Ravens U, Sanguinetti MC, eds. *Heart Rate and Rhythm*. Berlin, Heidelberg: Springer Berlin Heidelberg; 2011:133–151.

[2] McNary TG, Sohn K, Taccardi B, Sachse FB. Experimental and computational studies of strain-conduction velocity relationships in cardiac tissue. *Prog. Biophys. Mol. Biol.* 2008;97(2-3):383–400.

[3] Sung D, Mills RW, Schettler J, Narayan SM, Omens JH, McCulloch AD. Ventricular filling slows epicardial conduction and increases action potential duration in an optical mapping study of the isolated rabbit heart. *J. Cardiovasc. Electrophysiol.* 2003;14(7):739–749.

[4] Mills RW, Narayan SM, McCulloch AD. Mechanisms of conduction slowing during myocardial stretch by ventricular volume loading in the rabbit. *Am. J. Physiol. - Hear. Circ. Physiol.* 2008;295(3):H1270–H1278.

[5] Prinzen FW, Peschar M. Relation between the pacing induced sequence of activation and left ventricular pump function in animals. *Pacing Clin. Electrophysiol.* 2002;25(4 Pt 1):484–98.

[6] *(In Press)* Pfeiffer ER, Tangney JR, Omens JH, McCulloch AD. Biomechanics of cardiac electromechanical coupling and mechanoelectric feedback. *J. Biomech. Eng.* 2014.

[7] McCulloch AD, Smaill BH, Hunter PJ. Left ventricular epicardial deformation in isolated arrested dog heart. *Am. J. Physiol.* 1987;252(1 Pt 2):H233–41.

[8] McCulloch AD, Smaill BH, Hunter PJ. Regional left ventricular epicardial deformation in the passive dog heart. *Circ. Res.* 1989;64(4):721–733.

[9] Omens JH, May KD, McCulloch AD. Transmural distribution of three-dimensional strain in the isolated arrested canine left ventricle. Am. J. Physiol. 1991;261(3 Pt 2):H918–28.

[10] Omens JH, MacKenna DA, McCulloch AD. Measurement of strain and analysis of stress in resting rat left ventricular myocardium. *J. Biomech.* 1993;26(6):665–76.

[11] Emery JL, Omens JH, McCulloch a D. Biaxial mechanics of the passively overstretched left ventricle. *Am. J. Physiol.* 1997;272(5 Pt 2):H2299–305.

[12] Zhang Y, Sekar RB, McCulloch AD, Tung L. Cell cultures as models of cardiac mechanoelectric feedback. *Prog. Biophys. Mol. Biol.* 2008;97(2-3):367–382.

[13] Tung L, Zhang Y. Optical imaging of arrhythmias in tissue culture. *J. Electrocardiol.* 2006;39(4 Suppl):S2–6.

[14] Camelliti P, Gallagher JO, Kohl P, McCulloch AD. Micropatterned cell cultures on elastic membranes as an in vitro model of myocardium. *Nat. Protoc.* 2006;1(3):1379–91.

[15] de Bakker JMT, van Capelle FJL, Janse MJ, et al. Slow conduction in the infarcted human heart. "Zigzag" course of activation. *Circulation*. 1993;88(3):915–26.

[16] Rohr S, Scholly D, Kleber AG. Patterned growth of neonatal rat heart cells in culture. Morphological and electrophysiological characterization. *Circ. Res.* 1991;68(114-130).

[17] Bursac N, Parker KK, Iravanian S, Tung L. Cardiomyocyte cultures with controlled macroscopic anisotropy: a model for functional electrophysiological studies of cardiac muscle. *Circ. Res.* 2002;91(12):e45e–54.

[18] Gopalan SM, Flaim C, Bhatia SN, et al. Anisotropic stretch-induced hypertrophy in neonatal ventricular myocytes micropatterned on deformable elastomers. *Biotechnol. Bioeng.* 2003;81(5):578–87.

[19] Camelliti P, McCulloch AD, Kohl P. Microstructured cocultures of cardiac myocytes and fibroblasts: a two-dimensional in vitro model of cardiac tissue. *Microsc. Microanal.* 2005;11(3):249–59.

[20] Lee AA, Delhaas T, McCulloch AD, Villarreal FJ. Differential responses of adult cardiac fibroblasts to in vitro biaxial strain patterns. *J. Mol. Cell. Cardiol.* 1999;31(10):1833–43.

[21] Lee AA, Delhaas T, Waldman L, MacKenna DA, Villarreal FJ, McCulloch AD. An equibiaxial strain system for cultured cells. *Am. J. Physiol.* 1996;271(4 Pt 1):C1400–8.

[22] Jacot JG, Raskin AJ, Omens JH, McCulloch AD, Tung L. Mechanotransduction in Cardiac and Stem-Cell Derived Cardiac Cells. In: Kamkin A, Kiseleva I, eds. *Mechanosensitivity of the Heart*. Dordrecht: Springer Netherlands; 2010:99–139.

[23] Samarel AM. Costameres, focal adhesions, and cardiomyocyte mechanotransduction. *Am. J. Physiol. - Hear. Circ. Physiol.* 2005;289(6):H2291–301.

[24] Horiguchi K, Kouki T, Fujiwara K, Kikuchi M, Yashiro T. The extracellular matrix component laminin promotes gap junction formation in the rat anterior pituitary gland. *J. Endocrinol.* 2011;208(3):225–32.

[25] Côté PD, Moukhles H, Carbonetto S. Dystroglycan is not required for localization of dystrophin, syntrophin, and neuronal nitric-oxide synthase at the sarcolemma but regulates integrin alpha 7B expression and caveolin-3 distribution. *J. Biol. Chem.* 2002;277(7):4672–9.

[26] Wang YG, Samarel AM, Lipsius SL. Laminin binding to β1-integrins selectively alters β1- and β2-adrenoceptor signalling in cat atrial myocytes. *J. Physiol.* 2000;527(1):3–9.

[27] Gordon LM, Sauerheber RD, Esgate JA. Spin Label Studies on Rat Liver and Heart Plasma Membranes: Effects of Membrane Fluidity. *J. Supramol. Struct.* 1978;9:299–326.

[28] Qin H, Kay MW, Chattipakorn N, Redden DT, Ideker RE, Rogers JM. Effects of heart isolation, voltage-sensitive dye, and electromechanical uncoupling agents on ventricular fibrillation. *Am. J. Physiol. - Hear. Circ. Physiol.* 2003;284(5):H1818–26.

[29] Warren MD, Spitzer KW, Steadman BW, et al. High-precision recording of the action potential in isolated cardiomyocytes using the near-infrared fluorescent dye di-4-ANBDQBS. *Am. J. Physiol. - Hear. Circ. Physiol.* 2010;299(4):H1271–81.

[30] Hirschy A, Schatzmann F, Ehler E, Perriard J-C. Establishment of cardiac cytoarchitecture in the developing mouse heart. *Dev. Biol.* 2006;289(2):430–41.

[31] Baker LC, Wolk R, Choi B-R, et al. Effects of mechanical uncouplers, diacetyl monoxime, and cytochalasin-D on the electrophysiology of perfused mouse hearts. *Am. J. Physiol. Heart Circ. Physiol.* 2004;287(4):H1771–9.

Chapter 3

Caveolae in Stretch-Dependent Cardiac Conduction Slowing

Introduction

It is well recognized that mechanical loading can affect cardiac myocyte electrophysiology, but the cellular mechanisms of cardiac mechanoelectric feedback (MEF) remain poorly understood.[1] One observable manifestation of MEF in the heart is stretch-induced conduction slowing[2,3] (SiCS). This phenomenon has been shown to occur in a variety of species and tissue preparations (reviewed by McNary, *et al.*[4]) and results in conduction slowing under acute physiologic loads. By slowing propagation, SiCS would be expected to facilitate reentry during acute changes in diastolic loading, such as postural change, and thereby exert a proarrhythmic influence in these contexts. Importantly, because SiCS has been observed in a number of large and small mammalian species, as well as non-mammalian vertebrates, across which myocardial electrophysiology varies considerably, it is probable that SiCS arises from some set of well-conserved cellular mechanisms.[4] Two leading candidates are: (1) induction of stretch-activated currents (SACs),[4] which are thought to reduce excitability by elevating resting membrane potential, and (2) increased sarcolemmal capacitance[3] that may be caused by addition of cell surface area[5] during mechanical loading.

Two lines of recent evidence suggest that membrane capacitance changes may be a key contributor to SiCS. First, Mills *et al.*[3] observed that general SAC blockade by gadolinium did not prevent SiCS in the isolated perfused rabbit heart. It was also found that stretch changes in the membrane space constant, which when analyzed quantitatively, implicated a large increase in cellular membrane capacitance (C_m). Second, Kohl and colleagues[5] used electron microscopy to observe that ventricular filling of the isolated rabbit heart caused myocyte membrane unfolding and incorporation of sub-sarcolemmal caveolae into the plasma

membrane, thus suggesting an ultrastructural basis for acute changes in cellular capacitance due to stretch.

Recent data also suggest that caveolae may act as key membrane mechanosensors across a broad range of cell types. Sinha *et al*.[6] showed that uniaxial stretch or osmotic swelling in endothelial, muscle, and caveolin-1-expressing HeLa cells causes a loss of caveolae at the cell surface membrane. They proposed that stretch-induced recruitment and flattening of caveolae buffers surges in membrane tension. Opening or flattening of caveolae above a critical membrane tension also agrees with computational models[7,8] of membrane bending mechanics. Along with the heart-specific ultrastructural unfolding data from Kohl,[5] these findings present the intriguing possibility that caveolae provide a critical structural mechanism for cardiac MEF in general, and for SiCS in particular.

To investigate this, we used caveolin-3 knockout (Cav3 KO) mice that lack caveolae in myocytes and pharmacological depletion of membrane cholesterol to disrupt caveolar structure and function in whole hearts, and isolated neonatal mouse ventricular myocytes (NMVMs). Specifically we tested the hypothesis that SiCS is mediated by changes in membrane capacitance that are dependent on caveolae recruitment. We found that Cav3 is required for stretch-dependent conduction slowing in both whole hearts and isolated myocytes, and that stretch-induced recruitment of caveolae to the sarcolemma greatly increases cell membrane capacitance.

METHODS

Animal Models for Tissue Studies

All animal experiments were performed in accordance with an animal use protocol approved by the University of California, San Diego Institutional Animal Care and Use Committee. Eight- to ten- week old Cav3 KO[9,10] and age-matched C57BL/6 mice were used for electron microscopy and whole heart optical mapping studies.

Pressure-Loaded Isolated Heart Studies

Hearts were isolated and Langendorff perfused as described previously.[2] Mice were administered an intraperitoneal injection of 100 units of heparin. They were sacrificed by cervical dislocation and the heart was excised and placed in ice cold, hyperkalemic arrest solution. The aorta was rapidly cannulated on a 20 gauge stainless steel cannula. A fluid-filled length of polyethelene tubing fitted onto a 20 gauge luer adapter was inserted into the left ventricular (LV) cavity through the pulmonary vein and mitral valve and a tie was secured around the opening of the pulmonary vein. The heart was transferred to a Langendorff perfusion apparatus. The heart was perfused with a heated (35-37°C), oxygenated (95% O2, 5% CO2) modified Krebs-Henseleit solution (24.9 mM $NaHCO_3$, 1.2 mM KH_2PO_4, 11.1 mM dextrose, 1.2 mM $MgSO_4$, 4.7 mM KCl, 118 mM NaCl, and 2.5 mM $CaCl_2$) at a constant pressure of 65-70 mmHg. Flow rate was monitored with an inline flow probe (Transonic Systems, Inc.). The heart was submerged in a heated optical bath chamber to maintain epicardial temperature.

The tube in the LV cavity was connected to a reservoir of warmed, oxygenated perfusate, and an in-line pressure transducer was used to monitor LV pressure. The LV filling pressure (LVP) was controlled by the height of the reservoir with respect to the heart.

Isolated Heart Optical Mapping

Langendorff perfused hearts were optically mapped to investigate the effects of ventricular pressure on action potential propagation. Once the heart was cannulated, the heart was submerged in a bath of warmed perfusate in a water-jacketed chamber with a window for optical access. Electrodes in the bath chamber provided a volume-conducted electrocardiogram that was monitored and recorded throughout the experiment. The heart was allowed to beat freely for a 15-minute equilibration period. Myocardium was stained with a bolus injection of the potentiometric fluorophore di-4-ANEPPS (8 ml, 3.25 μM) into the perfusion line. The LV epicardium was excited with a light-emitting diode array (LEDtronics, Torrance, CA) at 470 nm. Fluorescence emission was collected by a custom-built tandem lens optical system (two 1x Plan APO macro objectives, Leica, Solms, Germany) filtered with >610 nm long-pass filter and focused onto a high-speed 14-bit CMOS camera (MiCAM Ultima L, SciMedia). Fluorescence images were acquired at 1000 frames per second and a spatial resolution of 100×100 pixels at 0.1 mm × 0.1 mm per pixel. The heart was paced at the lateral left ventricular midwall with a platinum unipolar electrode coated with Teflon except at the tip. A 2-ms rectangular constant current stimulus was applied at two times threshold and a cycle length of 200 ms, delivered by a digital stimulator (DS8000 stimulator and DLS100 isolator, World Precision Instruments, Sarasota, FL). Data were acquired in the unloaded state before loading with an LVP of 0 mmHg to measure baseline conduction velocity. The ventricular pressure was increased to 30 mmHg via the tube in the LV cavity for 1 minute and data was acquired at this loaded state. Finally, the LVP was returned to 0 mmHg and data was acquired in this unloaded state after loading. No chemical or mechanical intervention was implemented to restrict motion. Images were imported into MATLAB and analyzed using

custom software as described previously.[2,3] Activation time was identified at each pixel at the maximum rate of change of fluorescence for each beat. Conduction velocity vector fields were calculated from the spatial gradients of activation time over the surface of the ventricle.[11] Conduction velocity magnitudes were calculated from these vector fields and an apparent maximum and minimum conduction velocity (CV_{max}, CV_{min}) were defined as the 95th and 5th percentile values in the regions of fastest and slowest conduction respectively.

Electron Microscopy

Mouse hearts were prepared for electron microscopy to investigate the effects of increased load on membrane morphology and caveolae. Hearts were fixed either at unstretched baseline, *i.e.* after cannulation and perfusion but without additional ventricular pressure loading; during loading to a LV pressure of 30 mmHg; or following loading to 30 mmHg for 1 min and subsequent unloading to 0 mmHg. One minute after the final load change, the perfusate was switched to a standard Karnovsky's fixative of 4% paraformaldehyde, 1.5% gluteraldehyde in 0.1 M cacodylate buffer while hanging until the contractions stopped. It was further fixed in fresh fixative prior to dehydration with ethanol and embedding in LX112 (Ladd, Willston, VT #21210) with a longitudinal orientation. 70 nm sections were counterstained with lead citrate and uranyl acetate, and examined on JEOL CX100 TEM scope. 10 micrographs at 4800× magnification and 10 at 6800× magnification were taken per heart at random from sections for quantization of plasma membrane effects. Total cardiomyocyte membrane length was measured manually for each micrograph with ImageJ (NIH open source software). Structures resembling caveolae were counted in each of the 6800× magnification images and identified as sub-sarcolemmal or visibly integrated into the sarcolemma. Total density of caveolae and their localization were quantified. Additionally,

the ratio of membrane length to absolute length was calculated in the 4800× magnification images to quantify slack membrane.

Stretch of Micropatterned Neonatal Murine Ventricular Myocyte (NMVM) Cultures

Polydimethylsiloxane (PDMS) tissue culture substrates were molded from silicon wafers. The silicon molds were patterned by photolithograpy, using SU-8 2005 negative photoresist (MicroChem Corp., Newton, MA) and a custom designed photomask (Advance Reproductions Corp., North Andover, MA), as described previously.[12,13] These were used to pattern microgrooves 10 μm wide, 10 μm apart and 5 μm deep in Sylgard 186 silicone elastomer (Dow Corning Corp., Midland, MI). Murine laminin (Sigma-Aldrich, St. Louis, MO) was adsorbed onto the PDMS using a ten-minute 350 nm wavelength ultraviolet radiation treatment. The substrate was rinsed twice with 1× phosphate-buffered saline (MediaTech, Manassas, VA) prior to plating cells.

The PDMS substrates were mounted onto custom biaxial stretching devices similar to those used in previous studies.[12,14,15] The stretch devices used in this study applied a homogeneous anisotropic biaxial strain field. The micropatterned silicone elastomer substrates were mounted into anisotropic biaxial stretch devices such that the maximum principle axis of stretch was directed parallel to the longitudinal axis of the cell culture. Following recordings in the unstretched state before stretch, a biaxial strain field of 14% Lagrangian strain parallel to the cell culture longitudinal axis and 3.6% perpendicular to it was applied for 5 minutes prior to stretched measurements, and subsequently reversed with 5 minutes of rest prior to unstretched measurements after stretch.

Neonatal murine ventricular myocytes (NMVMs) were isolated from P1-P2 CD-1 mouse pups (Charles River Labs) using methods adapted from standard protocols.[16] Hearts were excised and enzymatically digested. Fibroblasts were removed from the cell suspension using a 90-minute pre-plating incubation and discarded. Cardiomyocytes were plated in the stretch device culture chambers in 15% serum plating media, and maintained at 37°C and 5% CO_2 for 2-4 days with media changes every 1-3 days. Cultures were maintained in standard 6% serum media until 24 hours prior to optical mapping experiments, when the media was changed to antibiotic-free media.

Optical Mapping of Micropatterned Monolayers

The stretch devices were mounted into an optical assembly for voltage mapping experiments. This method utilizes high temporal and spatial resolution imaging of a transmembrane voltage-sensitive fluorescent dye and avoids the electrical disturbances of electrode measurements.[17,18] The device is configured such that the culture substrate is maintained in the same position relative to the camera during loading and unloading. The imaging chamber was maintained at 37°C and cells were electrically stimulated at 300 ms intervals for the duration of the experiment.

Changes in voltage were detected using voltage-sensitive transmembrane fluorescent probe di-8-ANEPPS (Life Technologies, Grand Island, NY), loaded at 30 μM in a solution of antibiotic-free media and 0.1% Pluronic F-127 (Life Technologies, Grand Island, NY). The dye solution was replaced with serum- and antibiotic-free imaging media prior to imaging. Antioxidants were added to the dye and imaging solutions at physiological levels to reduce

ROS generation by the fluorescent probe.[19] 100 μM ascorbic acid (Fisher Scientific, Waltham, MA) and 450 μM uric acid (Sigma-Aldrich, St. Louis, MO) were added to each solution.

A 470-nm wavelength LED was used to excite the di-8-ANEPPS for electrophysiological measurement. Excitation light was directed to the cell culture substrate with a dichroic mirror, and emitted light passed through a 610 nm long-pass filter and was detected at 500 frames per second by a MiCAM Ultima-L CMOS camera. Depolarization was assessed according to time of maximum rate of fluorescence change at each pixel. The velocity of propagation of 5-6 consecutive, stimulated, and smoothly propagating action potentials per condition was measured along the longitudinal and transverse axes of the cell culture. Conduction along the same region relative to the pace site was compared for baseline, stretched and unstretched measurements.

Myocyte Patch Clamp

Individual NMVMs were patch-clamped on stretch-devices that were sparsely seeded so as to prevent cell coupling within 3 days of isolation. Borosilicate pipettes were 2-7 MΩ when filled with (in mM) 120 K-aspartate, 10 KCl, 10 NaCl, 5 Mg-ATP, 1 $MgCl_2$, and 0.3 Li-GTP (pH 7.2, KOH), and immersed in the bath solution (mM: 140 NaCl, 4 KCl, 1 $CaCl_2$, 1 $MgCl_2$, 10 D-glucose, and 10 HEPES; pH: 7.4, NaOH). An Axopatch 200B amplifier was used to apply 7 voltage steps of 200 ms between -120 and -60 mV (at 10 mV increments) from each of 5 holding potentials between -100 and -60 mV (again in 10 mV increments). For all steps, cell membrane capacitance (C_m) was calculated by standard approximation: $C_m = (Q + i_\infty \bullet \tau)/\Delta V$, where Q is the integral of the measured current above the steady state value (i_∞), τ is the time constant of current decay, and ΔV is the size of the voltage step. This approximation[20]

accounts for the exponential resistive component of the current response. Importantly, reported capacitances were taken from transients during -60 to -70 mV voltage steps (i.e. from the negative going phases of the -70 mV step at -60mV holding potential, and the -60 mV step from -70 mV holding potential). This was done to avoid contamination by I_{Na}, which was induced by the depolarizing phase of the steps in many NMVMs, and to further minimize error in the capacitive estimate due to I_{K1}-mediated changes in membrane resistance (R_m), which are exaggerated at more negative potentials.[21] Reported R_m values were taken from the negative-going steps between -80 and -90 mV, which is similar to the range of resting or maximum diastolic potential in these preparations.[22] This range of potentials also allowed more reliable R_m measurement, because at more positive potentials i_∞ was small enough (high R_m) to limit resolution of the signal (7 pA near resting potential versus 3 pA at more positive potentials). Cell membrane electrical time constants (T_m) were calculated from the product of C_m and R_m.

Lipophilic Dye

NMVMs were plated on micropatterned substrates for stretch, and incubated with 5 μM Vybrant DiO lipophilic dye (Molecular Probes, Life Technologies, Grand Island, NY) for 3 days from plating. Fluorescence was excited using a Lambda DG-4 fluorescent light source and captured with Photometrics Cascade 512F camera using MetaMorph v6.1 acquisition software. Fluorescent intensity per unit cell area was measured in the same cells before and immediately after 14% longitudinal by 3.6% transverse stretch, in both sham-operated and operated stretch experiments. 3-4 operated observations were conducted alongside and normalized to 1-2 sham observations, with every observation consisting of 6-20 cell measurements.

Statistics

Calculations were performed in MATLAB, Excel, and SigmaPlot. Measurements are reported as mean ± SEM. 1- and 2-way analyses of variance were conducted as regular or repeated measures where appropriate. If the data did not satisfy a Kolmogorov-Smirnov test of normality or a Levene Median test for equal variance, a generalized linear model nonparametric test was used. All analyses of variance were followed by Tukey pairwise multiple comparison procedures. Values of $P<0.05$ were accepted as statistically significant.

RESULTS

Mouse Ventricular Action Potential Propagation is Slowed by Increased Ventricular Filling Pressure Independently of SAC Blockade

Epicardial activation isochrones (**Fig. 3.1A**) showed that fastest conduction (CV_{max}) in the epicardially-paced wild-type (WT) mouse LV was approximately parallel to the epicardial fiber direction, with slowest conduction (CV_{min}) along the perpendicular axis. At zero left ventricular filling pressure (LVP), mean CV_{max} was 1.8- to 2.7-fold faster (653±15 $mm.s^{-1}$) than mean CV_{min} (311±26 $mm.s^{-1}$) as seen in **Fig. 3.1A**. The mean anisotropy ratio of conduction (CV_{max} / CV_{min}) did not vary significantly from before loading (2.2±0.2) to loaded (2.1±0.2, P=N.S.), as such, maximum epicardial conduction velocity (CV_{max}) is described in the remaining results except where stated otherwise. When LVP was increased from zero to 30 mmHg in the isolated heart, epicardial conduction slowed significantly within one minute by 19±5% ($P<0.01$) (**Fig. 3.1B**). After LVP was returned to 0 mmHg, conduction velocity

returned to 104±2% of baseline (P=N.S. *vs.* baseline, P<0.01 *vs.* loaded). Conduction velocities at each loading condition are plotted per heart in **Fig. 3.1C**.

Conduction in unloaded hearts perfused with the non-selective stretch activated channel (SAC) blocker gadolinium (Gd^{3+}, 50 μM) was, at 458±45 $mm.s^{-1}$, 30% slower on average than in untreated hearts (N=5, P<0.01 *vs.* untreated). However, SAC blockade with Gd^{3+} did not attenuate conduction slowing (to 340±55 $mm.s^{-1}$) due to LV pressure loading (P<0.01) (**Fig. 3.2**).

Conduction Slows Reversibly and Independently of SAC Blockade with Physiological Stretch in Micropatterned Neonatal Mouse Ventricular Myocyte Monolayers

Velocity of action potential conduction averaged from 5-6 consecutive paced action potentials in unstretched WT cultures was 1.2- to 7.2-fold (mean ratio 3.2±0.7) faster along the longitudinal axis of patterned myocytes (325±30 $mm.s^{-1}$) than in the transverse direction (124±22 $mm.s^{-1}$) (**Fig. 3.1D**). The mean anisotropy ratio of conduction did not vary significantly from before stretch (3.2±0.7) to stretched (2.9±0.6, P=N.S.). Maximal (longitudinal) CV is described in remaining results except where noted. As seen in **Fig. 3.1E**, conduction velocities in micropatterned neonatal murine cardiomyocytes cultures slowed acutely during stretch (26±4%, P<0.001). Five minutes after reversal of stretch, CV_{max} recovered to 90±5% of initial values (P<0.05 vs. baseline, P<0.01 from stretched) (**Fig. 3.1F**).

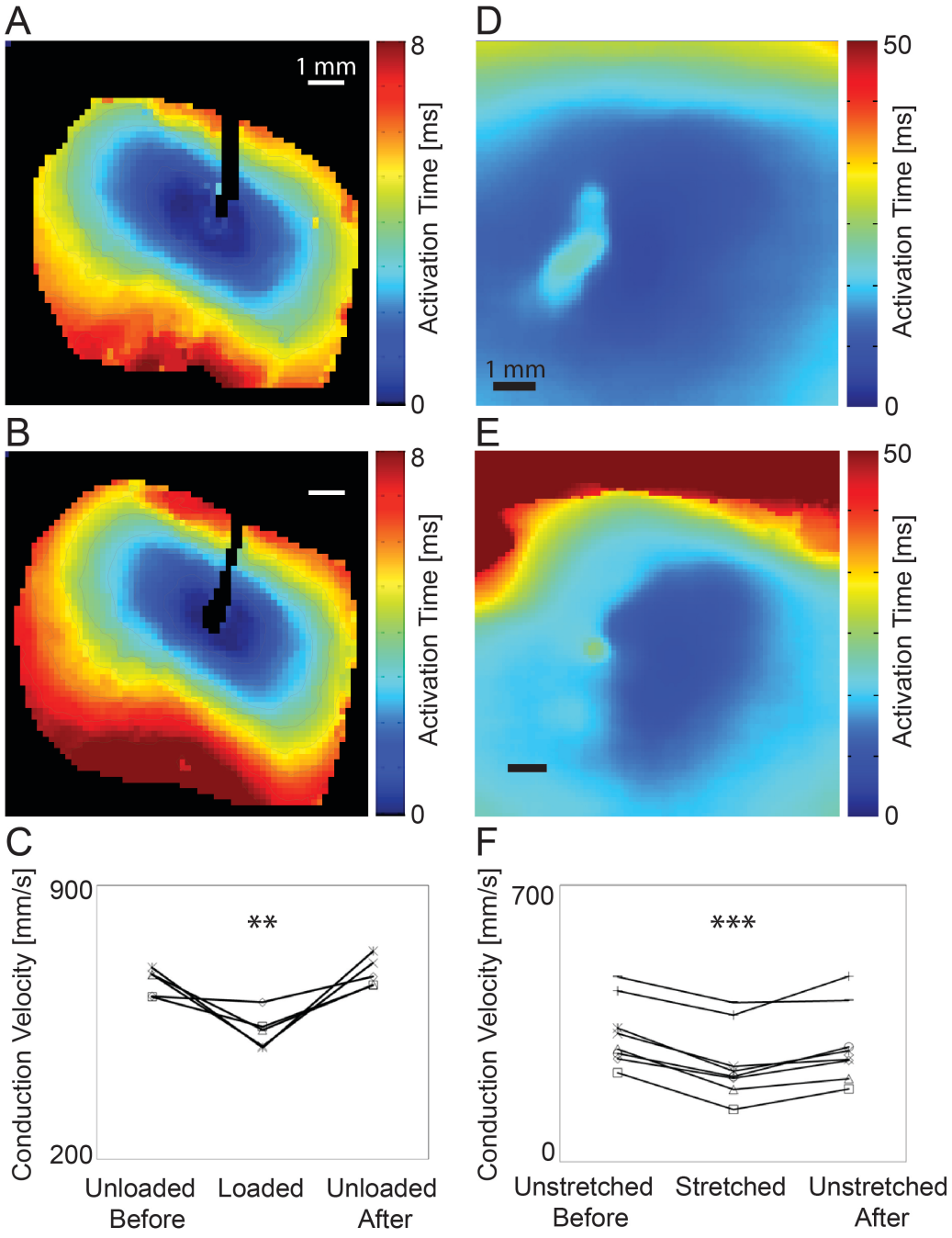

Figure 3.1: Effects of stretch on conduction velocity measured by fluorescence optical mapping in isolated hearts (A-C) and in micropatterned cardiomyocytes (D-F). Isochronal maps from the epicardium of an isolated WT mouse heart before (A) and after (B) ventricular pressure loading and from micropatterned neonatal ventricular myocyte cultures before (D) and after (E) anisotropic stretch show prolongation of activation times indicating conduction slowing during mechanical loading (scale 1 mm). Maximal epicardial conduction velocity (CVmax) in isolated mouse hearts (C) decreased significantly and reversibly during loading (N=5, **P<0.01). Maximal conduction velocity (CVmax) in cultured myocytes (F) decreased significantly and reversibly with stretch (N=8, ***P<0.001).

30-minute pre-incubation with the specific SAC blocking peptide GsMTx-4 (3 μM, kindly supplied by Dr. Frederick Sachs, SUNY Buffalo, NY) did not significantly alter the effects of stretch on CV, as seen in **Figure 3.2**. Though GxMTx-4 increased CV in unstretched cultures (1017±343 $mm.s^{-1}$, N=3, P<0.01 vs. untreated), stretch still significantly decreased CV in GsMTx-4-treated cultures (P<0.001).

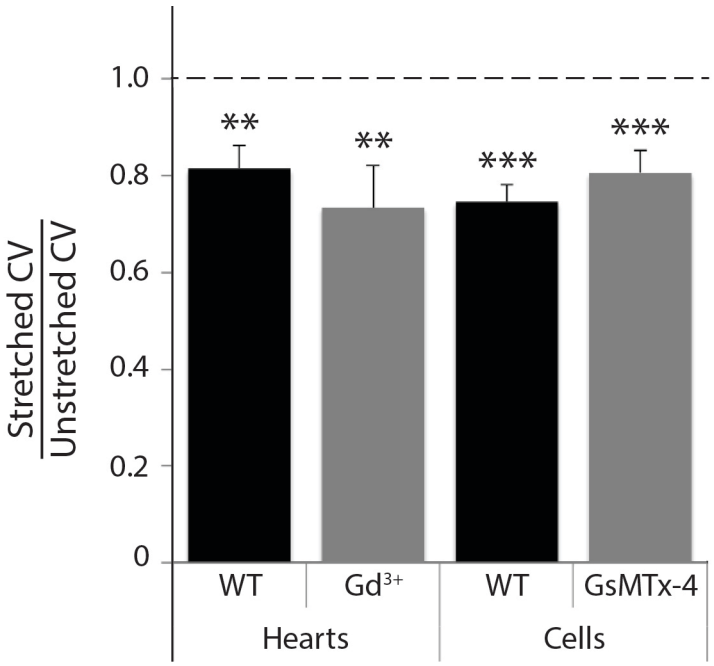

Figure 3.2: Conduction slowing with stretch is not affected by stretch-activated channel blockade in isolated hearts or myocytes. Mean conduction velocity in mechanically loaded hearts and cells was 70-80% of unstretched values in untreated hearts (N=5, P<0.01), hearts with stretch-activated channel blockade by Gd^{3+} (N=5, P<0.01), untreated cells (N=8, P<0.001), and in cells with stretch-activated channel blockade by peptide GsMTx-4 (N=3, P<0.001 cells).

Caveolae are Required for Stretch-Induced Conduction Slowing in the Isolated Heart and Micropatterned Myocyte Cultures

Depletion of caveolae attenuated conduction slowing during LV pressure loading. WT hearts perfused for 15 minutes with methyl-β-cyclodextrin (MβCD, 1 mM) (Sigma-Aldrich, St. Louis, MO), which depletes caveolae by sequestering cholesterol,[23] did not have significantly altered unloaded CV (692±16 $mm.s^{-1}$) compared with untreated hearts, as shown in **Figure 3.3A**, (N=5, P=N.S.). Conduction velocities observed in Cav3 KO hearts in the unloaded state (591±21 $mm.s^{-1}$) were not significantly different from those in unloaded WT hearts (N=5, P=N.S.) (**Fig. 3.3A**). There was no significant change in CV with load in Cav3 KO or MβCD-treated hearts (P=N.S.).

In micropatterned cultures of ventricular cardiomyocytes isolated from neonatal Cav3 KO mice, CV in unstretched conditions was not significantly different (503±96 $mm.s^{-1}$) than in WT cells (P=N.S., N=3), but there was no significant change in CV during stretch of Cav3 KO mouse myocyte cultures (553±83 $mm.s^{-1}$, P=N.S.) (**Fig. 3.3B**) indicating that Cav3 is required for stretch-dependent conduction slowing *in vitro*.

Hence acute stretch-dependent conduction slowing was absent both in hearts and cardiomyocyte monolayers from Cav3 KO mice, and in WT hearts treated with MβCD.

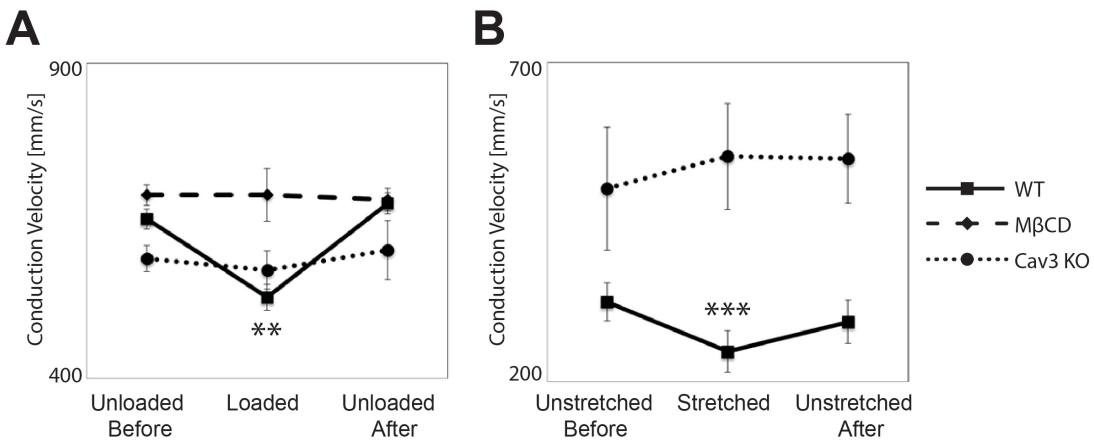

Figure 3.3: Stretch-dependent conduction slowing requires caveolae in isolated mouse hearts (A) and cultured myoctes (B). (A) Conduction slowing observed with loading in WT hearts is not seen when caveolae are depleted via either treatment with MβCD or genetic deletion of caveolin-3 (**WT hearts N=5, P<0.01; MβCD-treated and Cav3 KO hearts N=5, P=N.S.). (B) Conduction slowing observed in WT cells is prevented when caveolae are depleted via genetic deletion of caveolin-3 (***WT cells N=8 P<0.001; Cav3 KO cells N=3, P=N.S.). Within paired observations, only untreated WT hearts and myocytes show statistically significant changes with stretch.

Stretch In Vitro Significantly Increases Whole Cell Capacitance, Independent of SACs

Patch clamp studies in micropatterned WT NMVMs showed that membrane capacitance (C_m) increased dramatically and significantly with stretch from 22±3 pF to 43±8 pF (N=30, P<0.001), as seen in **Figure 3.4A**. SAC blockade using 3 μM GsMTx-4 for 30 minutes did not alter this effect (16±2 pF in unstretched cells *vs.* 40±4 pF in stretched cultures, N=19, P<0.01.).

Caveolae are Required for Stretch-Dependent Increase in Membrane Capacitance and Time Constant

Cell membrane capacitance was not significantly altered in cells treated with 1 mM MβCD for 30 minutes (12±1 pF, N=18, P=N.S. *vs.* WT), but stretched C_m was significantly

lowered relative to untreated cells (25±4 pF, N=22, P<0.01 *vs.* WT). MβCD treatment inhibited but did not fully block the increase in membrane capacitance during stretch (13±4 pF, P<0.05). However, genetic ablation of caveolae did completely block the effect of stretch on C_m. The mean increase in C_m with stretch in myocytes from Cav3 KO mice was only 3±4 pF (P=N.S., N=25) (**Fig. 3.4A**).

There were no significant changes with stretch, treatment or between genotypes in membrane resistance. However, membrane electrical time constants shown in **Figure 3.4B** increased almost four-fold in WT cells during stretch (from 20±6 ms to 78±26 ms, P<0.01). GsMTx-4 treatment did not significantly alter either unstretched (29±5 ms, P=N.S.) or stretched (62±22 ms, P=N.S.) time constants from WT. In MβCD-treated and Cav3 KO myocytes, unstretched time constants were not significantly different from WT (21±4 ms and 22±12 ms, respectively, P=N.S.), but stretched time constants were significantly smaller (25±5 ms and 23±12 ms, respectively, P<0.01 and P<0.05, respectively), and there was no significant increase in either with stretch (P=N.S.). Therefore, caveolae depletion alters cell membrane electrical time constant, while SAC-block does not.

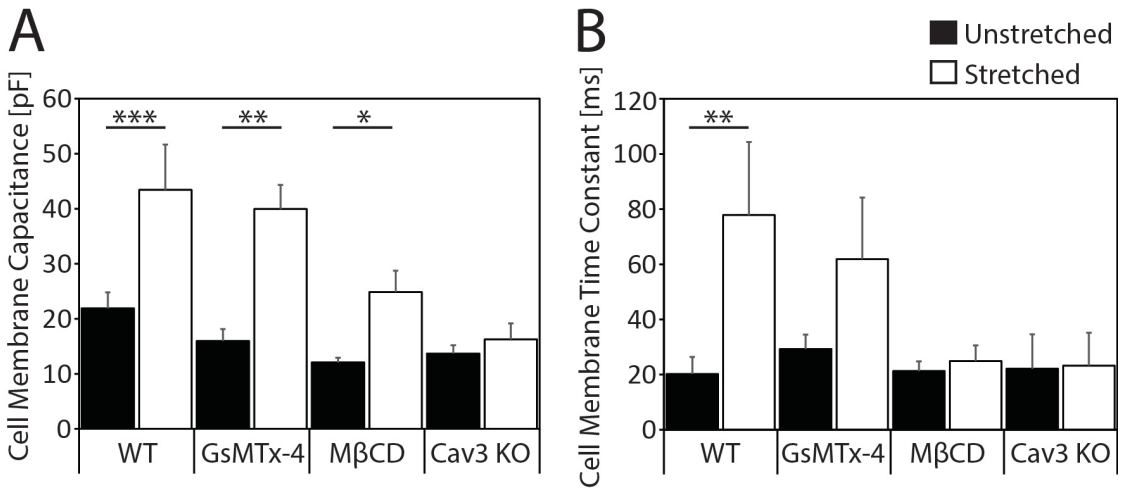

Figure 3.4: Cell membrane capacitance increases with stretch in a caveolae-dependent manner, resulting in a stretch-dependent and caveolae-dependent increase in membrane time constant. (A) Patch clamp recordings of sparsely-plated, micropatterned NMVMs significantly increased membrane capacitance with stretch in WT (N=15,15, ***P<0.001) and GsMTx-4-treated (N=11,8, **P<0.01) myocytes. There was a 41% smaller increase in MβCD-treated (N=18,22, *P<0.05) myocytes, and no significant change with stretch in Cav3 KO myocytes (N=13,12, P=N.S.). (B) There was a significant stretch-dependent increase in membrane time constant in untreated WT myocytes (**P<0.01), a doubling of time constant in GsMTx-4 treated WT myocytes (P=N.S.), and no significant change in MβCD-treated and Cav3 KO myocytes (P=N.S.).

LV Pressure Loading Smoothes Membrane Folds and Reduces Subsarcolemmal Caveolae

Electron microscopy revealed significant changes in gross membrane conformation and in the density and localization of caveolae with increased ventricular pressure load (**Fig. 3.5A**). The ratio of membrane length to absolute length (ML/AL) was measured as a quantification of slack membrane folds (**Fig.s 3.5A** and **3.5B**). In the pressure-loaded WT heart, the ML/AL ratio decreased from 1.140±0.019 in the unloaded state to 1.025±0.004 in the loaded state (P<0.001). In the WT heart fixed after load had been applied and removed, the average ML/AL ratio was 1.162±0.022 (P=N.S. *vs.* the initial measurement). In MβCD-treated hearts, the average ML/AL ratio was 1.094±0.010 in the unloaded preparation (P=N.S. compared with WT) and was also significantly reduced in the loaded state (1.046±0.009, P<0.01 *vs.* unloaded MβCD-treated). ML/AL was not significantly different between the

unloaded Cav3 KO heart and the unloaded WT heart (1.178±0.026, P=N.S.) but was significantly reduced in the pressure-loaded Cav3 KO heart (1.051±0.008, P<0.001 *vs.* unloaded Cav3 KO).

Electron microscopy confirmed that caveolae density was significantly diminished by either pressure-loading, or by interventions (MβCD-perfusion, Cav3 KO) intended to deplete caveolae. (**Fig. 3.5C**). In WT hearts, total caveolae density (**Fig. 3.5D**) was significantly lower in the pressure loaded heart (0.78±0.11 caveolae/μm) compared to the unloaded heart (1.23±0.14, P<0.05) or heart fixed after load had been applied then removed (1.27±0.10, P<0.05 *vs.* loaded, P=N.S. *vs*. unloaded). The density of caveolar structures in the unloaded MβCD-perfused and Cav3 KO hearts were 0.42±0.4 and 0.12±0.02 caveolae/μm respectively, as shown in **Fig. 3.5E**, significantly fewer than in the unloaded WT heart (1.23±0.14 caveolae/μm, P<0.001 for both).

Pressure-loading recruited caveolae away from the sub-sarcolemmal space in WT (**Fig. 3.5D**). In the unloaded heart, 0.95±0.09 and 0.29±0.06 caveolae/μm were observed in the sub-sarcolemmal and sarcolemmal categories, respectively. In the loaded heart, there were significantly fewer caveolae per membrane length in the sub-sarcolemmal space (0.44±0.07 caveolae/μm, P<0.001 *vs.* unloaded) and a slight but not significant increase in the density of caveolae fused with the membrane (0.34±0.05 caveolae/μm, P=N.S. *vs.* unloaded). The WT heart that was pressure-loaded and then unloaded prior to fixing revealed caveolae density and localization similar to the original unloaded heart (1.05±0.09 sub-sarcolemmal and 0.22±0.03 sarcolemmal caveolae/μm; P=N.S., compared with the initial measurement). All electron microscopy statistical comparisons use unpaired t-tests.

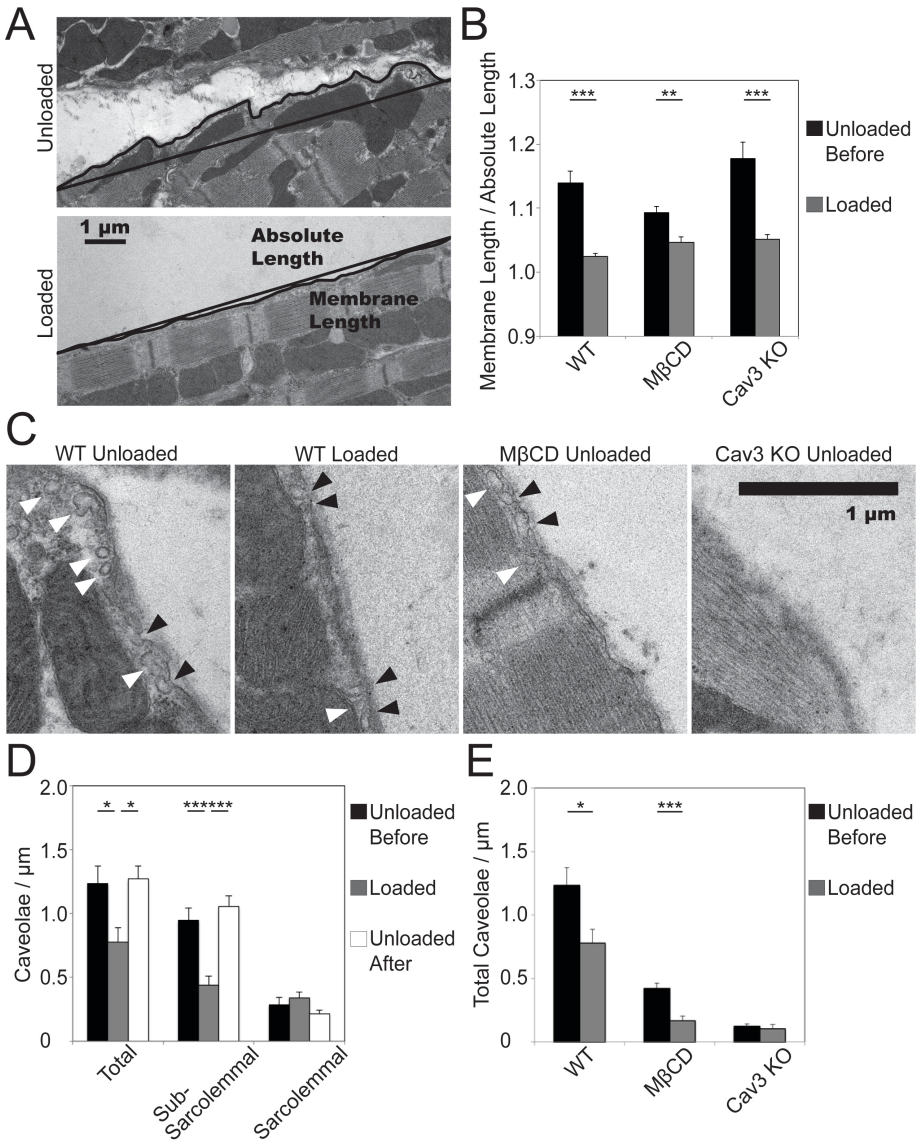

Figure 3.5: Stretch unfolds myocyte membrane and reversibly recruits sub-sarcolemmal caveolae in loaded hearts. Caveolae are reduced after treatment with MβCD or genetic deletion of caveolin-3. (A) Membrane is flattened during pressure loading (lower micrograph) compared with unloaded (upper micrograph), (scale: 1 µm). (B) Membrane length-to-absolute length ratio was reduced in the loaded vs. unloaded WT ($P<0.001$), MβCD-treated ($P<0.01$), and Cav3 KO ($P<0.001$) hearts. (N=10 images per condition, unpaired t-tests). (C) Sub-sarcolemmal caveolae (white arrows) and caveolae fused with the sarcolemma (black arrows) in the unloaded and loaded WT hearts, and the unloaded Cav3 KO and MβCD-treated hearts (scale: 1 µm). (D) Caveolae are reversibly recruited from the WT sub-sarcolemmal region during loading ($P<0.001$). (E) Total caveolae density is reversibly lower in the loaded state than before or after loading in WT. Caveolae in unloaded MβCD-treated hearts are less frequent than in WT ($P<0.001$), and are reduced ($P<0.001$) during loading. Caveolae are almost completely absent ($P<0.001$) in Cav3 KO hearts. (N=10 images per condition, unpaired t-tests).

Sarcolemmal Lipid Density Increases with Stretch in a Caveolae-Dependent Manner

Cells labeled with lipophilic fluorescent tracer showed a caveolae-dependent increase in fluorescent density with stretch (**Fig. 3.6**). In WT cells, fluorescent intensity per area relative to sham-handled cells increased nearly two-fold with stretch, from 0.80±0.12 to 1.57±0.20 (N=9, P<0.01). There was a significant interaction effect (P<0.05) and no significant change in Cav3 KO cells, which registered at 1.03±0.33 in unstretched and 1.00±0.32 in stretched relative to sham (N=4, P=N.S.).

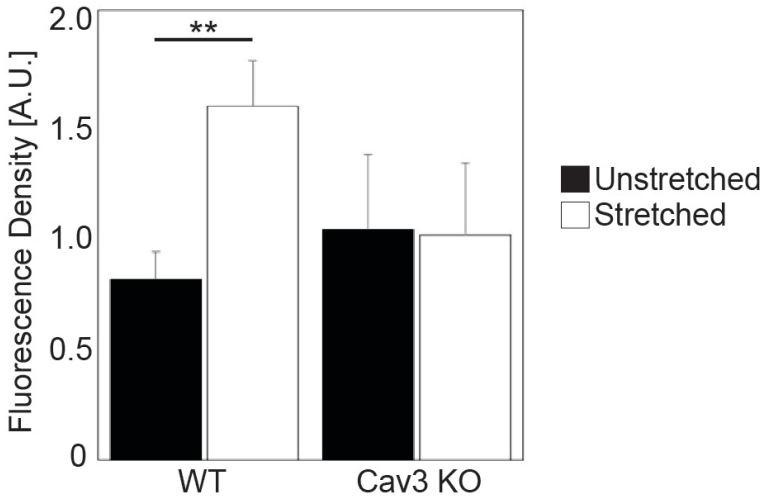

Figure 3.6: Stretch is associated with significant Cav3-dependent increase in lipophilic fluorescence density. Fluorescent intensity per cell unit area, normalized to sham, doubled with stretch in WT experiments (N=9, P<0.01) and showed no significant change in Cav3 KO cells (N=4, P=N.S.).

DISCUSSION

Mechanoelectric feedback is a known player in arrhythmia susceptibility; however, much of our understanding to date is focused on alterations in reverse excitation-contraction coupling and constituent ionic currents.[24,25] This study demonstrates stretch-dependent

slowing in cardiac conduction that is insensitive to stretch-activated current inhibition, but driven by an increase in membrane capacitance with stretch that requires intact caveolae.

A role for caveolae in cardiac mechanoelectric feedback has been hypothesized in a study demonstrating that caveolae are recruited and integrated into the sarcolemma of cardiomyocytes with stretch, suggesting that caveolae may modulate electrophysiology through enrichment of subpopulations of ion channels or signaling receptors, increased t-tubular convection, or by addition of cell area which would impact cell excitability.[5] Conduction slowing via a stretch-dependent increase in cell membrane capacitance is consistent with analysis of conduction slowing with ventricular filling in isolated, perfused rabbit hearts.[3] Capacitance has been observed to increase under various conditions of membrane tension in a range of cell types.[26] Given that changes in cell membrane capacitance have also been used as an index to measure caveolae and t-tubule expression,[30] a role for caveolae in altering conduction through changes in cell membrane capacitance is logical.

We used two model systems to probe the mechanisms of conduction mechanosensitivity: (1) isolated, perfused mouse hearts isolated from the autonomic nervous system, and (2) biaxially stretched micropatterned[12] murine cardiomyocyte monolayer cultures. The rationale for using the mouse heart model under conditions similar to demonstrations of conduction slowing in the rabbit heart[2,3] is the existence of transgenic models for deletion of proteins of interest. The micropatterned culture system extends this benefit in a condition of controlled biaxial stretch, free of interstitial effects, amplifying the ability to probe cellular electrophysiological mechanisms using precise optical and patch clamp techniques.

We observed that similar levels of conduction slowing occurred in isolated, pressure-loaded murine cardiac tissue, without the use of any mechano-electrical uncoupling reagents or mechanical restraint, and in a multi-cellular monolayer preparation subjected to biaxial stretch. This unique micropatterned cell culture and stretching platform was developed to determine the nature cardiomyocyte stretch-specific changes.[12,13,14,15,27] The platform separates changes in myocyte conduction via cardiomyocyte-intrinsic and stretch-dependent mechanisms from any effects of stretch on interstitial electrical properties, fluidic shear, or, as in the isolated heart preparation, extra-cardiac signals (e.g. autonomic, adrenergic). In addition, the 3 (or 2.5) dimensional substrate cues (extracellular matrix and structural support) provided by these microgrooves prevent the over-spreading culture artifact typically observed in flat tissue culture, thereby reducing artifacts in sarcolemmal biophysics. Perhaps as a consequence of the physiological myocyte shape and coupling arrangements guided by the micropatterned substrate, the cardiomyocytes in these preparations developed caveolae at a density similar to native tissue. Structures resembling immature t-tubules are also observed. This represents an advance over traditional tissue culture techniques on smooth, often glass, surfaces, in which t-tubules are often absent,[28] and expression of caveolae and t-tubules often decreases with time in culture[29] (although this effect may be less pronounced in mouse models than in rat[30]). This indicates that microstructured culture substrates may be an optimal system for study of the effects of cell membrane ultrastructure on multi-cellular cardiomyocyte electrophysiology. The biaxial stretch regime implemented more closely resembles physiological cardiomyocyte stretch than do uniaxial, osmotic, or shear stress applications, an important consideration when comparing *in vitro* studies to organ-level observations.[31,32]

Limitations

One limitation of these findings is that the study of SACs is a rapidly evolving field, and few drugs specifically targeting hypothesized mechanosensitive channels exist. However, the use of two different SAC-blocking agents in this study with similar results partially assuages this limitation. Taken together with this study, a panel of three different SAC blocking agents (streptomycin,[2] gadolinium,[3] GsMTx-4 peptide) have been tested in four models (isolated rabbit heart pressure loaded conduction,[2,3] isolated mouse heart pressure loaded conduction, stretched NMVM monolayer conduction, stretched single NMVM cell membrane capacitance, resistance, and time constant), with no significant alteration of stretch-dependent CV slowing or C_m increase detected with any compound. The three reagents named represent a panel including the currently most selective and historically widely used reagents available to intervene against SACs.

It may be observed that ion current effects outside non-specific cation-selective currents were not explored. Non-specific cation-selective SACs (SACns), targeted by GsMTx-4, Gd^{3+} and streptomycin, have been hypothesized to contribute to cardiac conduction slowing by reducing excitability through elevating resting membrane potential.[4] Another mechanism put forward for stretch-effects on ion currents is the insertion of either potassium and chloride,[33,34] or unknown mechanosensitive[35] channels at the cell surface via recruitment of caveolae. However, when observed in a cardiac setting, these observations of resulting changes in conductance were observed in atrial but not ventricular cells,[33] and were driven by either fluid shear which is generally low in the myocardium,[33] or by patch suction or probe indentation (through approximately 50% or more of cell diameter) in isolated myotubes[35] only. A role for SACs in altering conduction at the tissue-scale has not been demonstrated. Conversely, the utility of SACs in conduction slowing is unlikely by some accounts, as some rate- and species-dependent models[1,4] predict SACs to increase excitability.[36]

The two models for probing whether caveolae mediate stretch-dependent conduction slowing each have advantages and disadvantages. Two interventions were used in this study to deplete caveolae in accordance with precedent: genetic deletion of caveolin-3 and incubation with cholesterol-sequestering agent MβCD. Caveolin-3 is a cholesterol binding protein expressed in muscles that is instrumental in shaping caveolae and in t-tubule genesis, and is implicated in myopathies including cardiomyopathies.[37,38,39] Isolated adult hearts and NMVMs isolated from Cav3 KO mice were used in this study. MβCD was used in hearts only, as the treatment reduced fluorescent signal from micropatterned cell preparations to a level barring measurement.

Caveolin-3 knock-out mouse lines provide a unique tool to assess the impact of cardiac caveolae on physiology.[9,10,40] While genetically precise, the mice have a global lifetime deletion of caveolin-3, which bears a hypertrophic cardiac phenotype in adults and could result in non-cardiac effects and some degree of compensation in adult mice.[37,39] Hypertrophic and other deleterious phenotype manifests typically at 6-9 months of age in Cav-3 KO mice. All of our studies were performed in mice at 8-12 weeks of age where cardiac function is not different from WT animals. Until development of these genetic tools, MβCD was the sole method for caveolae depletion and remains widely used today. While the cholesterol-sequestering reagent may have effects on membrane biophysics beyond depleting caveolae, the MβCD approach presents an acute intervention which complements the genetic model.

Observations of increased propensity for arrhythmia have been made in other cav3 mutant mouse lines, and caveolin-3 mutations have been detected in patient populations. The

potassium ion channel Kv11.1 (ERG1), but not a long-QT associated mutant of the channel, localize to cholesterol- and sphingolipid-enriched microdomains including caveolae.[41] Additionally, depletion of membrane cholesterol using MβCD was observed to accelerate the kinetics of the channel, potentially a capacitance-driven effect.[41] Similarly, a caveolin-3 mutation has been linked to long-QT syndrome through increasing a late sodium current through a channel normally located in caveolae.[42] These and other studies of the electrophysiological implications of caveolae may be extended to account for the effects of altered cell membrane capacitance.

Cholesterol sequestration using MβCD might also give insight into the mechanism by which caveolae contribute to such a large increase in capacitance with stretch. Studies have indicated that insertion of cholesterol and other sterols in a plasma membrane increases lipid packing density, reducing proton and cation leak currents by a factor of three at physiologic concentrations of cholesterol when compared to lipid bilayers lacking sterols.[43] Those findings suggest a role for cholesterol in maintaining membrane pH and electrochemical gradients against passive currents, and our current study demonstrates a role for cholesterol-rich caveolae in augmenting membrane electrochemical capacitance during stretch, with physiologically meaningful slowing effects on cardiac conduction.

It should be noted that the two-fold increase in capacitance we observed is greater than the 60% effective capacitance increase estimated for conduction slowing,[3] and is greater than the expected cell area change with stretch. Though the effect of addition of caveolar material outweighs the area of the material, the effect of caveolae cholesterol-rich content could surpass the effect of contribution of area, as described above. The two-fold increase in lipophilic dye fluorescence we saw mirrors the increase in cell membrane capacitance, which

could either indicate a greater than expected recruitment of cholesterol-rich cell membrane material, or altered fluorescent properties of the dye molecule when the contents of caveolae are integrated into the sarcolemma.

Disproportionate effects of cholesterol-rich membrane material (rafts) associated with caveolae and t-tubules on cell membrane capacitance have been reported. Reports of skeletal muscle cell membrane capacitance using a glycerol infusion technique for disconnecting t-tubules have calculated two-fold higher (4 $\mu F.cm^{-2}$) membrane capacitance in the t-tubule system than in the surface plasma membrane, which itself measured two-fold higher (2 $\mu F.cm^{-2}$) than expected for the cell membranes of less caveolae-rich cells (0.7-1 $\mu F.cm^{-2}$).[44] This finding concurs with capacitive transients recorded in Purkinje fibers, which suggested a 2.4 $\mu F.cm^{-2}$ cell surface capacitance, compared with a 7 $\mu F.cm^{-2}$ element suggested to be the t-tubular network.[45] T-tubules, which are also enriched in caveolin-3, may contain as much as four-fold more cholesterol than the plasma membrane.[37] Our findings that cholesterol sequestration and caveolin-3 deletion lower baseline cell membrane capacitance by approximately 40% support the idea that mechanically-dynamic, caveolae-rich cell types have an elevated cell membrane-capacitance. The absence of the usual contributions of Cav3 to trafficking and concentrating cholesterol at the cell membrane[46] may, in this context, explain the faster baseline conduction velocities in the Cav3 KO NMVMs. While no significant difference was observed in the adult Cav3 KO hearts, this could be explained by the availability of circulating cholesterol to replenish membrane cholesterol[47] (but not caveolae) in cardiomyocytes. MβCD treatment also raised conduction velocity in hearts, but this difference was not significant, perhaps due to cholesterol replenishment through non-caveolar pathways.

In conclusion, these data support a caveolae-dependent mechanism for stretch-slowing of conduction in which caveolae are recruited to the sarcolemma with stretch and thereby increase cell membrane capacitance. This increased capacitance is due in part to addition of membrane material to the sarcolemma by recruitment and integration of caveolae, but is likely augmented by the particular content of the caveolar material. Stretch-activated ion currents do not appear to contribute significantly to conduction slowing. The effective increase in cardiomyocyte membrane capacitance via caveolae delays depolarization, slowing cardiac conduction. Such findings have implications for therapeutically targeting cardiac arrhythmias with caveolin- or caveolae-enhancement based approaches.

Acknowledgements

Chapter 3 is an almost exact reproduction of a manuscript in preparation for publication. The title and authors of the manuscript are as follows: E.R. Pfeiffer,* A.T. Wright,* A. Edwards, J.C. Stowe, K. McNall, J. Tan, I. Niesman, H.H. Patel, D.M. Roth, J.H. Omens, A.D. McCulloch. Caveolae in stretch-dependent cardiac conduction slowing. We gratefully acknowledge the contribution of peptide GsMTx-4 from Dr. Fred Sachs in Buffalo, NY, and technical assistance of Barbara Murienne, Michael Yang, Kyle Buchholz, Tammy Soo-hoo, Tik-Chee “Jenny” Cheng, and Mathivadhani Panneerselvam, and the animal management of Selma Garcia and others in the laboratory of Professors Roth and Patel and VA San Diego Hospital vivariums, as well as in the UCSD vivariums. Microfabrication of molds for PDMS patterning was carried out in the Nano3-Calit2 cleanroom facility at UCSD.

References

[1] Quinn TA, Bayliss RA, Kohl P. Mechano-electric feedback in the heart: effects on heart rate and rhythm. In: Tripathi ON, Ravens U, Sanguinetti MC, eds. *Heart Rate and Rhythm*. Berlin, Heidelberg: Springer Berlin Heidelberg; 2011:133–151.

[2] Sung D, Mills RW, Schettler J, Narayan SM, Omens JH, McCulloch AD. Ventricular filling slows epicardial conduction and increases action potential duration in an optical mapping study of the isolated rabbit heart. *J. Cardiovasc. Electrophysiol.* 2003;14(7):739–749.

[3] Mills RW, Narayan SM, McCulloch AD. Mechanisms of conduction slowing during myocardial stretch by ventricular volume loading in the rabbit. *Am. J. Physiol. - Hear. Circ. Physiol.* 2008;295(3):H1270–H1278.

[4] McNary TG, Sohn K, Taccardi B, Sachse FB. Experimental and computational studies of strain-conduction velocity relationships in cardiac tissue. *Prog. Biophys. Mol. Biol.* 2008;97(2-3):383–400.

[5] Kohl P, Cooper PJ, Holloway H. Effects of acute ventricular volume manipulation on in situ cardiomyocyte cell membrane configuration. *Prog. Biophys. Mol. Biol.* 2003;82(1-3):221–227.

[6] Sinha B, Köster D, Ruez R, et al. Cells respond to mechanical stress by rapid disassembly of caveolae. *Cell*. 2011;144(3):402–413.

[7] Kosawada T, Inoue K, Schmid-Schönbein GW. Mechanics of curved plasma membrane vesicles: resting shapes, membrane curvature, and in-plane shear elasticity. *J. Biomech. Eng.* 2005;127(2):229.

[8] Sens P, Turner MS. Budded membrane microdomains as regulators for cellular tension. *Phys. Rev. E*. 2006;73(3):031918.

[9] Oshikawa J, Otsu K, Toya Y, et al. Insulin resistance in skeletal muscles of caveolin-3-null mice. *Proc. Natl. Acad. Sci.* 2004;101(34):12670–5.

[10] Horikawa YT, Patel HH, Tsutsumi YM, et al. Caveolin-3 expression and caveolae are required for isoflurane-induced cardiac protection from hypoxia and ischemia/reperfusion injury. *J. Mol. Cell. Cardiol.* 2008;44(1):123–30.

[11] Bayly P V, KenKnight BH, Rogers JM, Hillsley RE, Ideker RE, Smith WM. Estimation of conduction velocity vector fields from epicardial mapping data. *IEEE Trans. Biomed. Eng.* 1998;45(5):563–71.

[12] Camelliti P, Gallagher JO, Kohl P, McCulloch AD. Micropatterned cell cultures on elastic membranes as an in vitro model of myocardium. *Nat. Protoc.* 2006;1(3):1379–91.

[13] Camelliti P, McCulloch AD, Kohl P. Microstructured cocultures of cardiac myocytes and fibroblasts: a two-dimensional in vitro model of cardiac tissue. *Microsc. Microanal.* 2005;11(3):249–59.

[14] Lee AA, Delhaas T, Waldman L, MacKenna DA, Villarreal FJ, McCulloch AD. An equibiaxial strain system for cultured cells. *Am. J. Physiol.* 1996;271(4 Pt 1):C1400–8.

[15] Zhang Y, Sekar RB, McCulloch AD, Tung L. Cell cultures as models of cardiac mechanoelectric feedback. *Prog. Biophys. Mol. Biol.* 2008;97(2-3):367–382.

[16] Sreejit P, Kumar S, Verma RS. An improved protocol for primary culture of cardiomyocyte from neonatal mice. *Vitr. Cell. Dev. Biol. - Anim.* 2008;44(3-4):45–50.

[17] de Bakker JMT, van Capelle FJL, Janse MJ, et al. Slow conduction in the infarcted human heart. "Zigzag" course of activation. *Circulation*. 1993;88(3):915–26.

[18] Tung L, Zhang Y. Optical imaging of arrhythmias in tissue culture. *J. Electrocardiol.* 2006;39(4 Suppl):S2–6.

[19] Warren MD, Spitzer KW, Steadman BW, et al. High-precision recording of the action potential in isolated cardiomyocytes using the near-infrared fluorescent dye di-4-ANBDQBS. *Am. J. Physiol. - Hear. Circ. Physiol.* 2010;299(4):H1271–81.

[20] Terracciano CMN, Harding SE, Adamson D, et al. Changes in sarcolemmal Ca entry and sarcoplasmic reticulum Ca content in ventricular myocytes from patients with end-stage heart failure following myocardial recovery after combined pharmacological and ventricular assist device therapy. *Eur. Heart J.* 2003;24(14):1329–1339.

[21] Zaniboni M, Cacciani F, Groppi M. Effect of input resistance voltage-dependency on DC estimate of membrane capacitance in cardiac myocytes. *Biophys. J.* 2005;89(3):2170–81.

[22] Nuss HB, Marbán E. Electrophysiological properties of neonatal mouse cardiac myocytes in primary culture. *J. Physiol.* 1994;479(2):265–79.

[23] Christian AE, Haynes MP, Phillips MC, George H. Use of cyclodextrins for manipulating cellular cholesterol content. *J. Lipid Res.* 1997;38:2264–2272.

[24] Calaghan SC, White E. Mechanical modulation of intracellular ion concentrations: mechanisms and electrical consequences. In: Kamkin A, Kiseleva I, eds. *Mechanosensitivity in Cells and Tissues*. Moscow: Academia; 2005:230–254.

[25] ter Keurs HEDJ. Electromechanical coupling in the cardiac myocyte; stretch-arrhythmia feedback. *Pflügers Arch. Eur. J. Physiol.* 2011;462(1):165–75.

[26] Morris C, Homann U. Cell surface area regulation and membrane tension. *J. Membr. Biol.* 2001;179:79–102.

[27] Gopalan SM, Flaim C, Bhatia SN, et al. Anisotropic stretch-induced hypertrophy in neonatal ventricular myocytes micropatterned on deformable elastomers. *Biotechnol. Bioeng.* 2003;81(5):578–87.

[28] Ibrahim M, Gorelik J, Yacoub MH, Terracciano CM. The structure and function of cardiac t-tubules in health and disease. *Proc. R. Soc. B Biol. Sci.* 2011;278(1719):2714–2723.

[29] Calaghan SC, Taggart MJ. Compartmentalized signaling in cardiomyocyte lipid domains--do structure and function match up? *J. Mol. Cell. Cardiol.* 2006;41(1):1–3.

[30] Pavlović D, McLatchie LM, Shattock MJ. The rate of loss of T-tubules in cultured adult ventricular myocytes is species dependent. *Exp. Physiol.* 2010;95(4):518–27.

[31] Jacot JG, Raskin AJ, Omens JH, McCulloch AD, Tung L. Mechanotransduction in Cardiac and Stem-Cell Derived Cardiac Cells. In: Kamkin A, Kiseleva I, eds. *Mechanosensitivity of the Heart*. Dordrecht: Springer Netherlands; 2010:99–139.

[32] [In Press] Pfeiffer E.R., Tangney J.R., Omens J.H., McCulloch A.D. Biomechanics of Cardiac Electromechanical Coupling and Mechanoelectric Feedback. *J Biomed Eng.* 2014.

[33] Kozera L, White E, Calaghan SC. Caveolae act as membrane reserves which limit mechanosensitive I(Cl,swell) channel activation during swelling in the rat ventricular myocyte. *PLoS One*. 2009;4(12):e8312.

[34] Boycott HE, Barbier CSM, Eichel C a., et al. Shear stress triggers insertion of voltage-gated potassium channels from intracellular compartments in atrial myocytes. *Proc. Natl. Acad. Sci.* 2013:1–10.

[35] Huang H, Bae C, Sachs F, Suchyna TM. Caveolae regulation of mechanosensitive channel function in myotubes. *PLoS One*. 2013;8(8):e72894.

[36] Kong C-R, Bursac N, Tung L. Mechanoelectrical excitation by fluid jets in monolayers of cultured cardiac myocytes. *J. Appl. Physiol.* 2005;98(6):2328–36.

[37] Le Lay S, Kurzchalia T V. Getting rid of caveolins: phenotypes of caveolin-deficient animals. *Biochim. Biophys. Acta*. 2005;1746(3):322–33.

[38] Al-Qusairi L, Laporte J. T-tubule biogenesis and triad formation in skeletal muscle and implication in human diseases. *Skelet. Muscle*. 2011;1:26.

[39] Fridolfsson HN, Patel HH. Caveolin and caveolae in age associated cardiovascular disease. *J. Geriatr. Cardiol.* 2013;10:66–74.

[40] Tsutsumi YM, Kawaraguchi Y, Horikawa YT, et al. Role of caveolin-3 and glucose transporter-4 in isoflurane-induced delayed cardiac protection. *Anesthesiology*. 2010;112(5):1136–45.

[41] Balijepalli RC, Delisle BP, Foell JD, Slind JK, Kamp TJ, January CT. Kv11.1 (ERG1) K+ channels localize in cholesterol and sphingolipid enriched membranes and are modulated by membrane cholesterol. *Channels*. 2007;1(4):263–272.

[42] Vatta M, Ackerman MJ, Ye B, et al. Mutant caveolin-3 induces persistent late sodium current and is associated with long-QT syndrome. *Circulation*. 2006;114(20):2104–12.

[43] Haines TH. Do sterols reduce proton and sodium leaks through lipid bilayers? *Prog. Lipid Res.* 2001;40(4):299–324.

[44] Gage P, Eisenberg R. Capacitance of the surface and transverse tubular membrane of frog sartorius muscle fibers. *J. Gen. Physiol.* 1969;53(3):265–278.

[45] Fozzard H. Membrane capacity of the cardiac Purkinje fibre. *J. Physiol.* 1966;182:255–267.

[46] Salanueva IJ, Cerezo A, Guadamillas MC, del Pozo M a. Integrin regulation of caveolin function. *J. Cell. Mol. Med.* 2007;11(5):969–80.

[47] Defesche JC. Low-density lipoprotein receptor—its structure, function, and mutations. *Semin. Vasc. Med.* 2004;4(1):5-11.

Chapter 4

Role of Desmoplakin in Multicellular Electrophysiology

Introduction

Cardiomyocytes are mechanically and electrically coupled at the intercalated disc (ICD) by gap junctions, desmosomes and fascia adherens components. Gap junctions provide a gateway for electrical conduction between cells, connexons, which are made up of connexin proteins, and are heavily remodeled in disease.[1] There is evidence that connexins are recruited to the ICD by components typically associated with mechanical adhesions (desmosomes, fascia adherens),[2] and for multiple interdependencies of protein localization between ICD components.[3] Alterations of connexin expression following increased ventricular mechanical loading suggest a potentially arrhythmogenic link between the mechanical and electrical coupling components of the ICD.[4,5] Mutations in desmosomal proteins such as desmoplakin and plakoglobin, have been linked with cardiac disease phenotypes, including ventricular arrhythmias such as arrhythmogenic right ventricular cardiomyopathy (ARVC).[6,7] However, there remain a number of open questions regarding the mechanisms of disease manifestation in these patients. For example, fibrofatty replacement of the ventricle is considered a hallmark of ARVC and has been widely postulated to be a key pathological factor that elicits the fatal arrhythmias; however, it is yet to be determined whether there is a direct and early mechanistic consequence of desmosomal (e.g., desmoplakin) deficiency on gap junction components and cell-cell coupling in a system independent of fibro-fatty manifestation. This is important to determine since a recent study suggested that electrophysiological abnormalities were thought to appear prior to fibro-fatty replacement of the myocardium in human ARVC patients carrying desmoplakin mutations and heterozygous desmoplakin deficient mice.[8]

In the current study, we tested desmosomal function using a novel mouse model of ARVC that is reminiscent of the postnatal onset of a biventricular form of human ARVC at the histological, physiological and electrophysiological levels. We provide evidence for desmoplakin as a direct stabilizer of connexin signaling, which includes the demonstration that loss of desmoplakin has direct mechanistic consequences on connexin-43 levels and phosphorylation, leading to conduction abnormalities prior to the molecular dissociation of the mechanical junction complex within a system that is independent of the fibro-fatty manifestation observed in ARVC.

We also investigated whether desmosomes play a role in tissue level pacemaking mechanisms. The cardiac pacemaker complex (PC) is a highly heterogeneous tissue. Understanding of pacemaker function has primarily focused on ion channel biology, essential the initiation action potentials. However, integral to pacemaker tissue architecture is the presence of connections at the cell-cell interface that include anchoring junctions such as desmosomes. The importance of cell-cell coupling for cardiac pacemaking remains poorly understood.

Methods

Cardiomyocyte-Specific Desmoplakin Knockout Mouse Lines

Desmoplakin floxed mice (kind gift from Dr. Elaine Fuchs, Rockefeller University)[9] and heterozygous ventricular myosin light chain-2 Cre mice (kind gift from Dr. Ju Chen, University of California-San Diego)[10] have been previously characterized, and were used to generate cardiomyocyte-specific desmoplakin floxed for knockout (DSP-cKO) mice. DSP-

cKO mice and their control littermates were kept in a congenic C57B/6 background. All animal procedures were in full compliance with the guidelines approved by the University of California–San Diego Animal Care and Use Committee. Ventricular cardiac myocytes were isolated from neonatal (1-2 day old) desmolplakin floxed mouse hearts and cultured on micropatterned substrates as described in **Chapter 2** and **Chapter 3**.

Adenoviral Infection of Cardiomyocyte Cultures

Adenovirus vectors containing the lacZ (AdLacZ) and Cre recombinase (AdCre) cDNAs were prepared (UCSD Viral Vector Core) and used at multiplicity of infections 1.6-12.5 pfu/cell. Neonatal ventricular cardiac myocytes isolated from desmoplakin floxed mice were plated on laminin and infected with AdLacZ and AdCre, two days following isolation, as previously described[11] and as illustrated in Figure 7A. Viral particle carrying medium was changed from cells after 24 hrs and cells were subsequently maintained in a media consisting of DMEM, M199, 5% fetal bovine serum, 10% Horse Serum and 1% Penicillin/ Streptomycin/Glutamine for the duration of the study. Cardiomyocytes were analyzed four days post-infection. Protein expression and localization was analyzed using standard western blot and immunofluorescent methods. In previous experiments, a significant 83 ± 5.6% (n=3) and 87 ± 4.3% (n=3) reduction in desmoplakin protein levels was observed in both total and insoluble (intercalated disc enriched) fractions, respectively, in DSP-cKO cardiomyocytes when compared with littermate controls. Immunofluorescence staining analyses of cardiac sections highlighted the dramatic loss of desmoplakin at the intercalated disc, which is delineated by the retained presence of N-cadherin, in DSP-cKO hearts, when compared to littermate hearts.[12]

Optical Mapping

Activation of cardiomyocyte cultures was optically mapped similarly to described in **Chapter 2** and **Chapter 3**. In studies of conduction, cultures were stimulated with a point electrode at either 100 ms or 300 ms intervals for conduction studies, though spontaneous activation events were not excluded. Cultures in which activation was conducted over less than 75% of the area observed were considered to exhibit conduction block. In several cases, the test was repeated on a cell culture paced at several unique locations to differentiate between conduction block and altered excitability. Maximum distances and areas of continuous activation front propagation without functional conduction block were measured in ImageJ (U. S. National Institutes of Health, Bethesda, MD), with attention given to maximum distances with respect to the longitudinal and transverse axes of cell culture and at an arbitrary angle, and maximum conducting area surrounding any initiation site. Of the experiments considered (n=8), one experiment included 2 replicates each of control (AdLacZ) and desmoplakin knock-down (AdCre) cultures, and two experiments included 3 AdCre replicates. In studies of interbeat interval (IBI), cultures were not stimulated and beat spontaneously. The intervals of time between successive spontaneous depolarizations were measured over 4 second recordings.

Statistical Analysis

Data presented in the text and figures are expressed as mean values ± SEM. Significance was evaluated by the 2-tailed Student's t test or repeated measures ANOVA. $P<0.05$ was considered statistically significant.

Results

Desmosomal Defects Contribute to Conduction Block

To determine the functional consequences of primary loss of desmoplakin levels on cardiomyocyte conduction, we optically mapped cardiac action potential propagation in an aligned neonatal mouse cardiomyocyte model system similar to described in **Chapter 2 and Chapter 3,** as a tool to examine desmoplakin deficient (AdCre) versus control (AdLacZ) cardiomyocyte cultures (**Fig. 4.1A**). Optical maps from cardiomyocyte cultures were obtained following pacing and evaluated for both total area as well as distance of action potential propagation along different paths (longitudinal, transverse, arbitrary) from the pacing electrode (**Fig. 4.1B**). Representative optical maps from AdCre and AdLacZ infected cardiomyocytes highlight that both the total area and distance of action potential propagation is markedly less in desmoplakin deficient versus control cardiomyocytes (**Fig. 4.1B**). Quantitative analyses of the distance of continuous propagation in both groups revealed that desmoplakin deficient cardiomyocytes display significantly reduced propagation across longitudinal, transverse and arbitrary angles when compared to control cardiomyocytes (**Fig. 4.1C**). We also show that desmoplakin deficient cardiomyocytes display a significantly reduced area of continuous propagation when compared to control cells, indicative of conduction block (**Fig. 4.1D**), suggesting that loss of desmoplakin has a direct impact on cardiac conduction, which is reflective of loss of connexin 43 function in a setting independent of fibrofatty manifestation associated with ARVC.

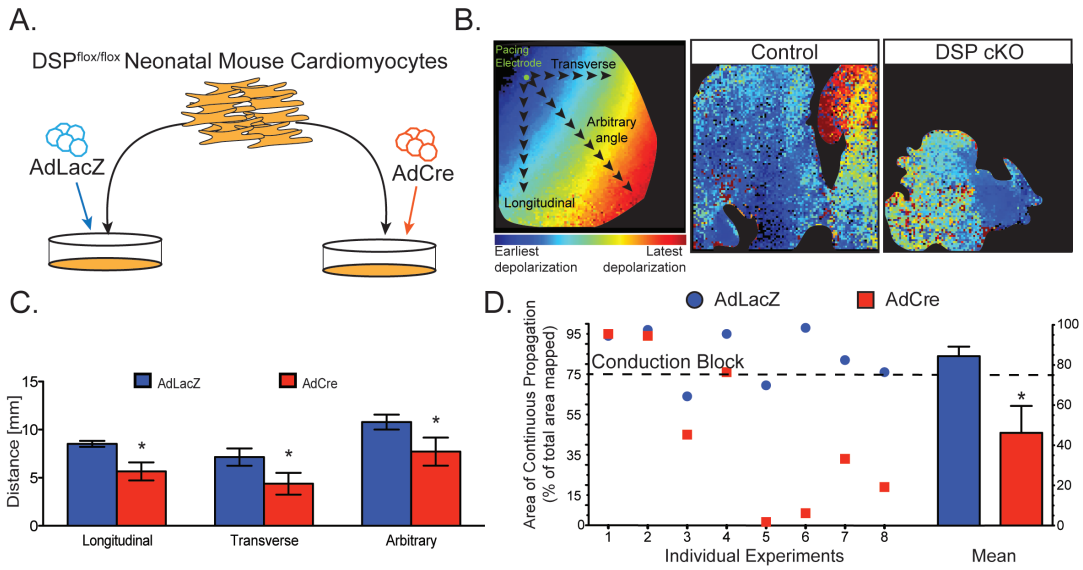

Figure 4.1: Desmoplakin knock-down leads to electrical conduction block in aligned neonatal mouse ventricular cardiomyocytes (NMVC). (A) Schematic representation of the strategy used to knock-down desmoplakin expression in NMVC isolated from $DSP^{flox/flox}$ mice. (B) Distances of continuous propagation were measured at longitudinal and transverse angles as well as at an arbitrary angle across the longest distance. Representative activation time plots from control (AdLacZ) and desmoplakin-deficient (AdCre) NVMC 4 days post-infection. (C) Quantification of distances of continuous propagation in control and desmoplakin-deficient NVMC. n = 8, *P < 0.05. (D) Quantification of the area of continuous propagation in control and desmoplakin-deficient NVMC. n = 8, *P < 0.05. An area of continuous propagation of <75% of the total area mapped was demonstrative of conduction block. Figure adapted from Lyon *et al.*[12]

The large imaging area in this preparation permits observation of regions capable of tissue-scale electrophysiological behavior, such as reentrant arrhythmia (**Fig. 4.2**). Multicellular phenomena such as reentry, or spiral waveforms, are characteristic of many human arrhythmias but are typically not able to be observed in the spatial scale – limited mouse model. The use of the model system described here allows study of transgenic mouse model cardiac electrophysiology at spatial scales similar to human tissue, increasing the capacity for clinically-applicable observations.

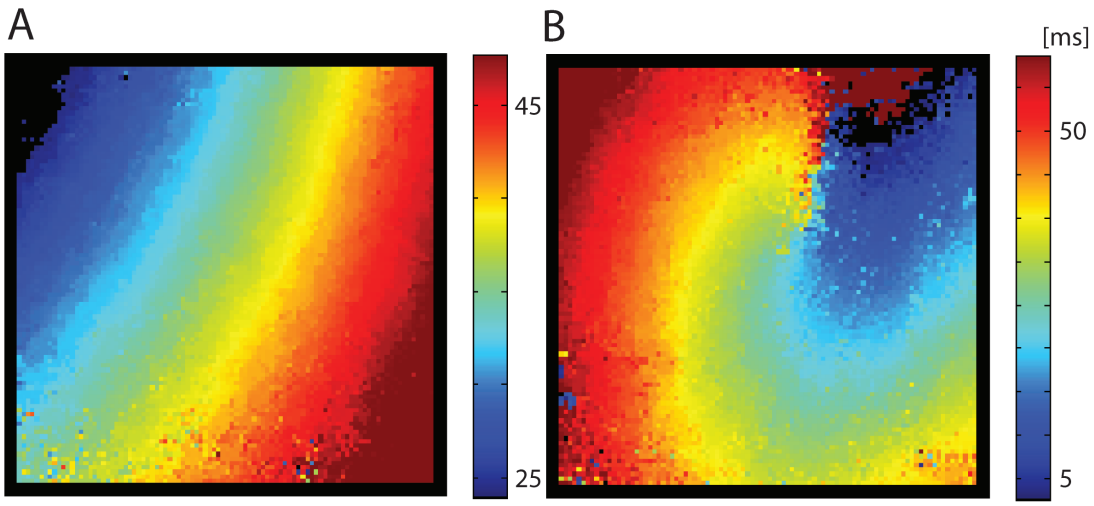

Figure 4.2: A spiral wave is observed in a DSPKO culture. A) Control with normal propagation. B) DSPKO with spiral wave propagation.

Mechanoelectric Uncoupling Influences Beat Rate Variation

The previous data suggests that removal of DSP might give rise to competition between the normally coordinated foci of leading pacemakers. We hypothesized that this might be due to an uncoupling of the PC both mechanical, through loss of desmosomes and, secondarily, electrical by loss or decrease of gap junctions. The tissue complexity of the PC makes testing our hypothesis in this system very challenging, we therefore used a tightly controlled in vitro system. Ventricular cardiomyocytes obtained from neonatal mice (NMVC) have spontaneous depolarization activity very much like pacemaker cells.[13] This feature provides a robust way to model pacemaker synchrony and coupling in an isolated, controlled system of thousands of cells. We measured the interbeat intervals of spontaneous depolarizations that occurred in a network of neonatal cardiomyocytes via optical mapping **(Fig. 4.3).** A representative experiment is shown in **Figure 4.3A** where the cycle length of each successive beat is graphed as an independent event. For control cells (AdLacZ, open circles) the cycle lengths were similar from one beat to the next, whereas in DSP KO cells

(AdCre, black circles) the cycle lengths varied considerably from one beat to the next as quantified by the coefficient of variation. Paired comparisons of control (AdLacZ) and DSP free cultures (AdCre) showed that even though the mean IBI did not significantly change (paired two-tailed t test p=0.0881, n=3 independent experiments) the coefficient of variation of the IBIs was significantly increased by removal of DSP (AdLacZ 11.78%, AdCre 35.2%, paired one tail t test p=0.0296, n=3 independent experiments **(Fig. 4.3B)**. The idea that in these cells electrical uncoupling might mediate the increase in IBI variability is in agreement with previous observations performed in chick and rat myocytes.[13,14]

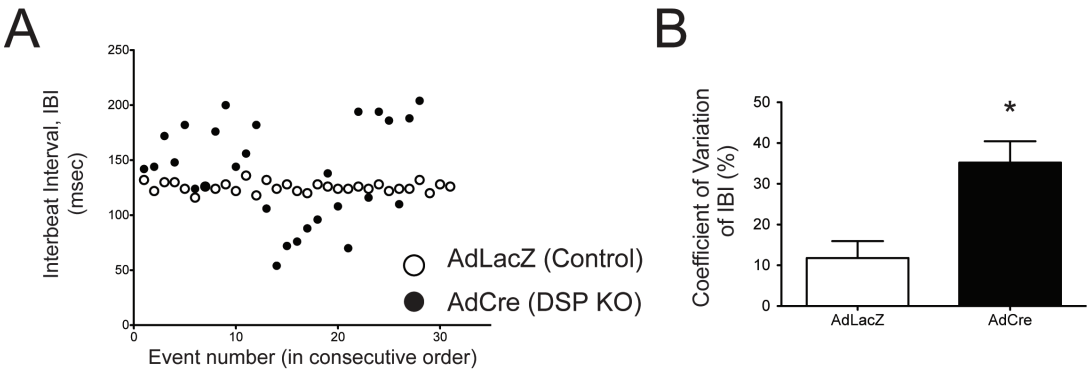

Figure 4.3: A) Representative set of consecutive interbeat intervals (IBI) measured via optical mapping of neonatal cardiomyocytes obtained from $DSP^{flox/flox}$ mice. IBI from cells infected with Control adenovirus (AdLacZ) and Cre-Recombinase expressing adenovirus (AdCre) in open and closed circles respectively. B) Coefficient of variation obtained from three independent experiments. *$p<0.05$, paired one-tailed t-test. C) Immunostaining of AdLacZ and AdCre infected cardiomyocytes form on eof the optical mapping experiments. Green: sarcomeric α-actinin, Red: plakoglobin, Blue: DAPI. Scale is 50 μm.

Loss of Desmoplakin Reduces Connexin 43 Expression, Phosphorylation and Function

The integrity of the tissue culture monolayer is maintained as demonstrated by staining for plakoglobin, an adherens junction protein (**Fig. 4.4A**). Yet, reduction in desmoplakin protein downregulates total and phosphorylated (S368) connexin-43 protein, prior to and independent of the molecular dissociation of the desmosomal and fascia adherens

junction complex, as evidenced by the robust levels of plakophilin-2 and N-cadherin in neonatal cardiomyocytes following desmoplakin knockdown (**Fig. 4.4B**). These results suggest that loss of desmoplakin has primary consequences on connexin-43 levels and the gap junction complex.

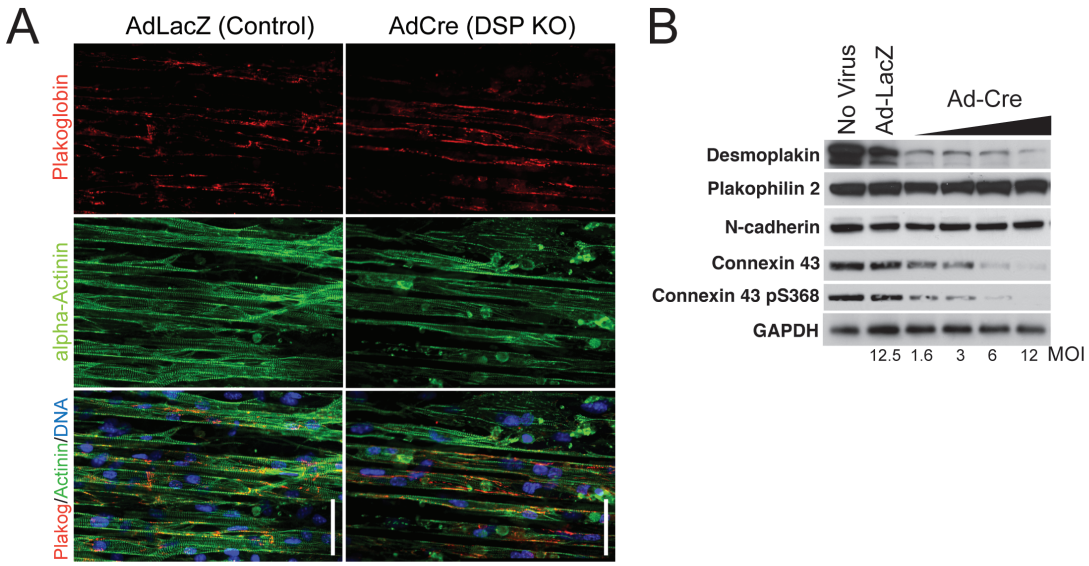

Figure 4.4: A) Immunostaining of AdLacZ and AdCre infected cardiomyocytes from one of the optical mapping experiments. Green: sarcomeric a-actinin, Red: plakoglobin, Blue: DAPI. Scale=50 µm. B) Western blot analysis of intercalated disc protein levels in viral infected cells was performed 4 days post-infection. GAPDH was used as a loading control. Figure adapted from Lyon *et al.*[12]

Conclusions

This study demonstrates the capabilities of optical mapping a micropatterned, multicellular platform in probing the cardiac electrophysiology of transgenic murine models of human disease, at spatial scales permitting development of phenomena reminiscent of human electrophysiology. The DSP-cKO model examined here serves as a tool for understanding the molecular mechanisms underlying ARVC.

The mechanical integrity of adhesions between cells can influence conduction and beat rate. Desmosomes secure firm mechanical coupling between neighboring cardiomyocytes, necessary to facilitate conduction of action potentials through expression and proximity of gap junction connexins. Loss of desmosomal coupling can lead to conduction block. The regularity of this coupling appears to influence beat rate, formerly thought to be modulated through pacemaker cell "clocks" and autonomic signaling.

We believe our studies further the understanding of PC function as an emergent property of the network of pacemaker cells in addition to uniformity of conduction. We hope to move the field beyond the ionic properties of isolated sinoatrial nodal or ventricular cells towards a coordinated network that is capable of integrating complex structural information at the tissue level.

Acknowledgements

Chapter 4 contains text and figures almost identical to two manuscripts, with formatting changes for this dissertation, along with additional original text and figures (Fig. 4.4). One has been accepted for publication and is in press at *Human Molecular Genetics* which is a publication of Oxford University Press. The citation is: Lyon, R.C.,* Mezzano, V.,* A.T. Wright, E. Pfeiffer, J. Chuang, K. Banares, A. Castaneda, K. Ouyang, L. Cui, R. Contu, Y. Gu, S.M. Evans, J.H. Omens, K.L. Peterson, A.D. McCulloch, F. Sheikh, 2013. Connexin defects underlie arrhythmogenic right ventricular cardiomyopathy in a novel mouse model. Human Molecular Genetics. The second manuscript is in preparation for submission to *Ciculation Research*, and the working title and authors are: V. Mezzano, A.T. Wright, R.C.

Lyon, E. Pfeiffer, Y. Gu, N. Dalton, S.M. Evans, K.L. Peterson, A.D. McCulloch and F. Sheikh. Desmosomal junctions are necessary for synchronized action potential propagation in the mouse cardiac pacemaker complex.

References

[1] Severs NJ, Bruce AF, Dupont E, Rothery S. Remodelling of gap junctions and connexin expression in diseased myocardium. *Cardiovasc. Res.* 2008;80(1):9–19.

[2] Palatinus J a, Rhett JM, Gourdie RG. The connexin43 carboxyl terminus and cardiac gap junction organization. *Biochim. Biophys. Acta*. 2011.

[3] Lim BK, Xiong D, Dorner A, et al. Coxsackievirus and adenovirus receptor (CAR) mediates atrioventricular-node function and connexin 45 localization in the murine heart. *J. Clin. Invest.* 2008;118(8):2758.

[4] Zhuang J, Yamada K a, Saffitz JE, Kléber AG. Pulsatile stretch remodels cell-to-cell communication in cultured myocytes. *Circ. Res.* 2000;87(4):316–22.

[5] Gopalan SM, Flaim C, Bhatia SN, et al. Anisotropic stretch-induced hypertrophy in neonatal ventricular myocytes micropatterned on deformable elastomers. *Biotechnol. Bioeng.* 2003;81(5):578–87.

[6] Sheikh F, Ross RS, Chen J. Cell-cell connection to cardiac disease. *Trends Cardiovasc. Med.* 2009;19(6):182–90.

[7] Delmar M, McKenna WJ. The cardiac desmosome and arrhythmogenic cardiomyopathies: from gene to disease. *Circ. Res.* 2010;107:700–714.

[8] Gomes J, Finlay M, Ahmed AK, Ciaccio EJ, Asimaki A, Saffitz JE, Quarta G, Nobles M, Syrris P, Chaubey S, McKenna WJ, Tinker A, Lambiase PD. Electrophysiological abnormalities precede overt structural changes in arrhythmogenic right ventricular cardiomyopathy due to mutations in desmoplakin-A combined murine and human study. *Eur. Heart J*. 2012;33:1942-1953.

[9] Vasioukhin V, Bowers E, Bauer C, Degenstein L, Fuchs E. Desmoplakin is essential in epidermal sheet formation. *Nat. Cell Biol.* 2001;3:1076-1085.

[10] Chen J, Kubalak SW, Chien KR. Ventricular muscle-restricted targeting of the RXRalpha gene reveals a non-cell-autonomous requirement in cardiac chamber morphogenesis. *Development* 1998;125:1943-1949.

[11] Sheikh F, Raskin A, Chu PH, Lange S, Domenighetti AA, Zheng M, Liang X, Zhang T, Yajima T, Gu Y, Dalton ND, Mahata SK, Dorn GW, Heller-Brown J, Peterson KL, Omens

JH, McCulloch AD, Chen J. An FHL1-containing complex within the cardiomyocyte sarcomere mediates hypertrophic biomechanical stress responses in mice. *J. Clin. Invest.* 2008;118:3870-3880.

[12] *(In Press)* Lyon RC, Mezzano V, Wright AT, Pfeiffer E, Chuang J, Banares K, Castaneda A, Ouyang K, Cui L, Contu R, Gu Y, Evans SM, Omens JH, Peterson KL, McCulloch AD, Sheikh F, 2013. Connexin defects underlie arrhythmogenic right ventricular cardiomyopathy in a novel mouse model. *Hum. Mol. Gen.*

[13] Rook MB, de Jonge B, Jongsma HJ, Masson-Pevet MA. Gap junction formation and functional interaction between neonatal rat cardiocytes in culture: A correlative physiological and ultrastructural study. *J Membr Biol.* 1990;118:179-192.

[14] Clay JR, DeHaan RL. Fluctuations in interbeat interval in rhythmic heart-cell clusters. Role of membrane voltage noise. *Biophys J.* 1979;28:377-389.

Chapter 5

Conclusion

Conclusion

In conclusion, multicellular preparations have been shown to be useful in studying cardiac electrophysiology, particularly mechanoelectric feedback. These preparations bridge the gap in understanding historically separating organ-level observations and single-cell recordings, reviewed in **Chapter 1**. While risk of arrhythmia is increased in diseases associated with altered cardiac mechanics, and multiple phenomena of MEF have been observed in intact hearts, it has proven difficult to determine underlying cell phenomena in intact heart preparations due to tissue heterogeneities and interstitial effects. Conversely, it has been difficult to predict the organ-level effects of recorded alterations in single-cell electrophysiology with stretch, without the context of physiologic cell-cell coupling.

An experimental preparation has been developed which addresses a significant need in the study of cardiac mechanoelectric feedback, as described in **Chapter 2**. These multicellular preparations provide well-coupled cardiomyocytes with physiologic morphology. Anisotropic conduction is observed, with longitudinal (fiber-parallel) conduction out-pacing transverse conduction approximately three-fold, a mark of maturity in development of cardiomyocyte junctions. When stretched, the multicellular preparations revealed two MEF phenomena of conduction velocity modulation by stretch: conduction speeding at small stretches (maximum stretch smaller than 5%) and conduction slowing at large stretches (maximum conduction larger than 10%). These phenomena appeared generally isotropic with regard to both stretch and conduction direction.

The cellular mechanisms for conduction slowing were probed in **Chapter 3.** Stretch-activated channel (SAC) block using TRPC channel mechanosensitivity inhibiting peptide

GsMTx-4 did not alter conduction slowing observed in multicellular preparations with acute 14%×3.6% stretch. Conduction slowing in hearts was similarly not reduced by SAC blocker Gd^{3+}. However, depletion of caveolae *via* genetic deletion of caveolin-3 in hearts and cells, or by depletion of cholesterol using MβCD in hearts, did prevent conduction slowing. Cell membrane capacitance was found to double with stretch in wild-type cells and cells treated with GsMTx-4, but this increase was reduced when caveolae were reduced by MβCD and no significant increase was observed in cells lacking caveolae due to deletion of caveolin-3. In observation of membrane ultrastructure by electronmicroscopy and membrane area by lipophilic dye, caveolae were observed to contribute membrane material to the sarcolemma during stretch. The stretch-dependent recruitment of material by caveolae is implicated as a mechanism for slowing conduction *via* increasing cardiomyocyte membrane capacitance, with observable effects in both multicellular preparations and in intact hearts.

The multicellular preparation is used to investigate the electrophysiological role of the desmosomal protein desmoplakin in **Chapter 4**. Desmoplakin is a component of the mechanoelectric coupling complex found at the intercalated disc. In studies of Cre recombinase-mediated knockdown of the protein, desmoplakin was found to be important in maintaining junctions necessary for conduction, its loss resulting in conduction block. Loss of uniform coupling, attributed to a role of desmoplakin in localizing connexin, also generated increased variation of beat rate.

In summary, the multicellular preparations here are useful in studying emergent mechanoelectric feedback phenomena that require physiologic morphology, coupling and stretch of populations of cardiomyocytes, on a spatial scale reflecting human physiology. In addition to identifying caveolae- and desmosomal-mediated electrophysiological phenomena,

these preparations hold promise in furthering understanding of multicellular electrophysiology.

Acknowledgements

The content of Chapter 5 is original. The author would like to thank Professors Andrew McCulloch and Jeffrey Omens for guidance in this project and Adam Wright, Valeria Mezzano and Andy Edwards for discussions of mechanoelectric feedback, intercellular coupling, and electrophysiology.